August 2022

# Properties of Titanium Dioxide Nanoparticles Aquesous Dispersions Stabilized By Anionic Surfactants

Anita Vuchkovska
*University of Wisconsin-Milwaukee*

# PROPERTIES OF TITANIUM DIOXIDE NANOPARTICLES AQUEOUS DISPERSIONS STABILIZED BY ANIONIC SURFACTANTS

by

Anita Vuchkovska

A Thesis Submitted in

Partial Fulfillment of the

Requirements for the Degree of

Master of Science

in Engineering

at

The University of Wisconsin-Milwaukee

August 2022

ABSTRACT

PROPERTIES OF TITANIUM DIOXIDE NANOPARTICLES AQUESOUS DISPERSIONS STABILIZED BY ANIONIC SURFACTANTS

by

Anita Vuchkovska

The University of Wisconsin-Milwaukee, 2022
Under the Supervision of Professor Konstantin Sobolev

The stability of titanium dioxide nanoparticles dispersed in aqueous solutions with and without anionic surfactants was investigated as a function of phase separation (sedimentation), particle size at the age of 3±3 and 30±3 days, polydispersity at 3±3 and 30±3 days, and zeta potential. Mechanical energy in the form of homogenization or mixing with propeller blade mixer was used to wet out the titanium dioxide ($TiO_2$) nanoparticles in the aqueous media and this process was evaluated for the capability of developing a stable dispersion. The ultrasonic waves were used as a second step to form stable dispersions. The research results indicated that the wetting out of the titanium dioxide nanoparticles using homogenization or mixing was not sufficient to develop a stable dispersion, and ultrasonic waves play crucial role in the initial and long-term stability of the dispersions. Furthermore, the effect of nanoparticle dispersion by homogenization or mixing was insignificant when ultrasonic waves were subsequently used. For the dispersed nanoparticles the absolute zeta potential was greater than 30 mV for eleven of the twelve formulas, with -47.40 being the greatest, indicating that a good stability was achieved during the dispersion process. The particle size did not increase significantly for the period from 3±3 days to 30±3 days. The polydispersity for all samples was between 0.12-0.23 and 0.13-0.24 at age 3±3 days and 30±3 days, respectfully, indicating a moderate polydispersed distribution.

The proposed dispersion method demonstrated a pathway for effective dispersion of nanoparticles for application in acidic (pH=4.00-4.10), near-neutral (pH=6.42-6.79), and basic (pH=9.23-10.52) systems.

TABLE OF CONTENTS

LIST OF FIGURES

LIST OF TABLES

LIST OF ABBREVIATIONS

| | |
|---|---|
| AFM | Atomic Force Microscope |
| AU | Arbitrary Units |
| BET | Brunauer, Emmett and Teller |
| DLS | Dynamic Light Scattering |
| DLVO | Derjaguin, Landau, Verwey, and Overbeek |
| eV | Electron Volt |
| FT-IR | Fourier Transform-Infrared Spectroscopy |
| IEP | Isoelectric Point |
| IUPAC | International Union of Pure and Applied Chemistry |
| NNI | National Nanotechnology Initiative |
| NP | Nanoparticles |
| PAA | Polyacrylic Acid |
| PCS | Photon Correlation Spectroscopy |
| PSD | Particle Size Distribution |
| RPM | Revolutions Per Minute |
| SHMP | Sodium Hexametaphosphate |
| STM | Scanning Tunneling Microscope |
| SEM | Scanning Electron Microscope |
| XRD | X-Ray Diffraction |
| QELS | Quasi Electric Light Scattering |
| QPA | Quantitative Phase Analysis |
| WPG | Weight Per Gallon |

ACKNOWLEDGEMENTS

I would like to express my sincere gratitude to Dr. Sobolev for his guidance and mentorship through my graduate studies. His passion for science, dynamism, vision, motivation, and incredible source of knowledge have deeply inspired and helped me see the science and engineering field from a different perspective. It has been a privilege and honor to study under his mentorship. Furthermore, I would like to thank Dr. Kozhukhova and Dr. Church for serving on my thesis committee, and for their valuable advice during my studies. I would also like to thank all past and current members of Sobolev Research Group for all their help, support, and friendship. Additionally, I would like to thank W. R. Meadows for their support and allowing me to have a flexible work schedule, so I can focus on my studies.

Finally, I would like to thank my parents, sisters, grandparents, and partner for their unconditional love and never-ending support. Without them, I would have never been here. I would especially like to express my sincere gratitude to my middle sister, Saska, for all her help, support, and encouragement.

# 1. Introduction

## 1.1 Nanomaterials and nanotechnology

The idea of nanotechnology had originated back in 1959 during the famous lecture "There is Plenty of Room at the Bottom" given by the Nobel Laureate Richard P. Feynman during a meeting of the American Physical Society at California Institute of Technology. During this meeting, Feynman introduced the concept of manipulating matter at the atomic level [1]. Since then, nanotechnology has been the driving force of a new industrial revolution. From discovering of the scanning tunneling microscope (STM) in 1981 by Binnig and Rohrer and discovering of nanocrystalline, semiconducting quantum dots in glass matrix by Ekhimov that same year, to the discovery of the Buckmisterfullerene (C60) by a group of scientists from Rice University in 1985 and to the invention of atomic force microscope (AFM) in 1986, the 1980's were years for experimental advances and inventions that set up the base for nanotechnology research and made it possible in the coming years, especially with the invention of the instruments that allow the scientists and researcher to observe the matter at the atomic level [2], [3]. In 1991, Iijima discovered the carbon nanotubes (needle-like tubes) [4] and in 1993 Bawendi invented a way to synthesize the nanocrystals under controlled conditions [2], [3]. Even though some early nanotechnology companies, such as Helix Energy Solution Group and Nan-Tex started to operate in the 1990's, nanotechnology application and utilization in consumer product did not begin until the early 2000's [2].

In 1974, Japanese scientist, Norio Taniguchi, first used the word "nano-technology" to describe the processes in semiconductors. He defined "nano-technology" as: "… processing of separation, consolidation, and deformation of materials by one atom or molecule" [5]. The National Nanotechnology Initiative (NNI) defined nanotechnology as: "…science, engineering

and technology that is done at the nanoscale level" [6]. When refereeing to nanoscale level and nanomaterials, the definition could slightly vary between different disciplines and industries. However, the references made to nanoscale and nanomaterials commonly deal with dimensions of materials between 1 and 100 nm. Due to their small size, nanomaterials, and nanostructures are of high importance because the mechanical, physical, and chemical properties are not dictated by the bulk but rather by their surface chemistry. As the size of materials decreases from bulk to nanoscale, the surface area to volume ratio and surface energy of nanomaterials increases. When the surface area increases releasing the atoms present at the surface, it leads to the increase in reactivity. These properties give the nanomaterials strong advantages over "traditional" or bulk materials. The properties of nanomaterials can be engineered and altered by controlling their size, shape, and synthesis during manufacturing [7].

Nanotechnology involves two different approaches: the top-down and the bottom-up approach. The top-down approach starts with bulk materials when size is reduced to a nanoscale using mechanical means where the properties of the bulk remain and there is no control at the atomic level, and therefore the particle size distribution (PSD) of particles is broader [7]–[9]. The bottom-up approach also known as molecular nanotechnology was introduced by Drexler where materials are expected to be engineered from atoms or molecules through assembly or self-assembly [8]. This approach can yield a narrower PSD, but dispersions produced this way are subjected to Ostwald ripening – a phenomena where small particle in solution dissolve and deposit on the surface of larger particles to get to lower energy state [9], [10]. The second method is of high importance in medicine, pharmacy, biotechnology, and energy sectors. Figure 1.1 provides a schematic summary of top-down and bottom-up approaches.

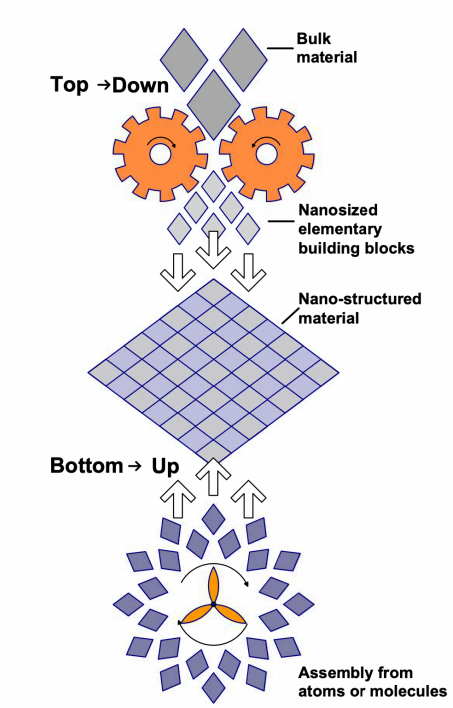


**Figure 1.1.1 – Top-down and bottom-up approaches** [11], [12]

Nanotechnologies have revolutionized many sectors in various industries. However, nanotechnology has not reached its full potential in the construction and building materials fields. One reason is the difficulty of dispersing and de-agglomerating the nanoparticles to get the optimum performance and associated benefits. The high surface area and surface energy that give advantage to nanomaterials over the traditional materials, are the same properties that disadvantage them and lead to agglomeration and aggregation. Nanomaterials agglomerate so they can reduce the surface energy and reach a lower energy state. Developing a stable dispersion of nanoparticles as finished products or precursors to be further utilized in coatings, treatments, and composites for the construction and building industry is of high importance to realize the optimum potential of the nanoparticles from performance and sustainability standpoint. It is well known that nanoparticles tend to agglomerate, so using of mechanical and

chemical means to disperse them and stabilize them to achieve a long-term stability is imperative for effective applications.

## 1.2 Colloidal nanoparticles (nanoparticle dispersions)

A colloid is a mixture where insoluble particles (dispersed phase) are dispersed in another medium (continuous phase). The particle size of the dispersed phase for colloids is 1 nm to 1 $\mu$m. For colloidal nanoparticles, the particle size of the dispersed phase is considered to be 1 – 100 nm. Some examples of colloidal dispersions are foams (gas/liquid), emulsions (liquid/liquid) and sols or dispersions (solid/liquid) [13], [14]. The particles in the dispersed phase and the continuous phase can be in a solid, liquid or gas state. All these combinations can form a colloid if the two phases are insoluble, except gas in gas (as these are miscible).

Sols – solid/liquid dispersions

Nanoparticle dispersions or colloidal nanoparticles are inherently unstable. From thermodynamic standpoint, the colloidal nanoparticles tend to agglomerate to reach a lower energy state. From attraction forces standpoint, the combination of van der Waals attraction forces and Brownian motion lead to agglomeration, aggregation and eventually phase separation, if the dispersions are not properly stabilized. To develop more stable dispersions, the attraction forces between the nanoparticles need to be reduced or the repulsive forces needs to be increased. Two known mechanisms for stabilization of nanoparticle dispersions or colloids are steric and electrostatic stabilization.

Steric stabilization also known as polymeric stabilization is a mechanism where solvable polymers or nonionic surfactants are absorbed on the surface of the nanoparticles creating strong repulsion forces between the nanoparticles to prevent the agglomeration and aggregation [15], [16].

Electrostatic stabilization is a mechanism where repulsive forces counterbalance the attractive van der Waals forces typically as a result of absorbed polyelectrolytes at the surface of the particle. A phenomenon known as electric double layer that is formed at the space of the nanoparticle-liquid interphase, plays a fundamental role when it comes to electrostatic stabilization. The electric double layer which is electrically neutral is a layer that surrounds the nanoparticles surface (dispersed phase) and includes ions absorbed at the surface of the nanoparticles and a film of the countercharge continuous phase (or dispersion medium). The electric double layer has three constituents: surface charge, Stern layer, and diffuse layer. The surface charge is usually negative in aqueous medias due to the high dielectric constant of water. The Stern layer has an opposite charge to the surface charge which is attracted to the particle surface by the electrostatic force. The diffuse layer which is a film of the continuous phase (dispersion medium) and has free ions with greater concentrations of the ions present at the Stern layer [15], [16]. The electrostatic stabilization is more common for the dispersions where the continuous phase is water or other highly polar solvent. Figure 1.2.2 provides a schematic representation of the electric double-layer concept.

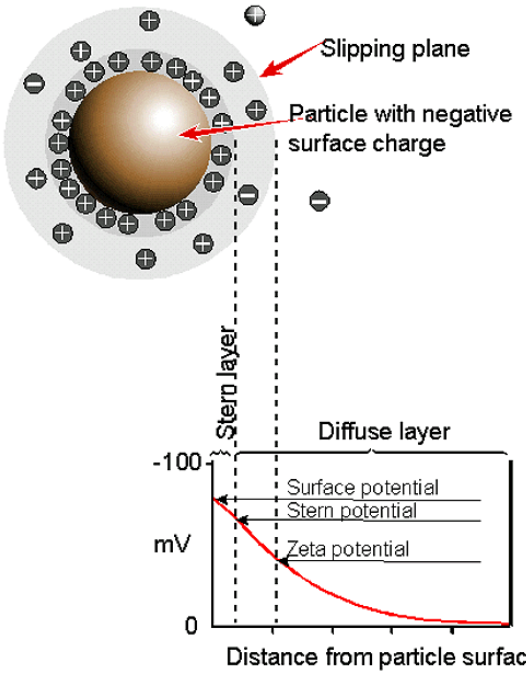


**Figure 1.2.1 – Schematic representation of electric double layer and zeta potential** [17]

As nanoparticles move in the dispersions, a small part of the surrounding liquid stays attached to them. The edge of this layer is known as shear plane or slipping plane. The electrical potential at the shear plane corresponds to the zeta potential – a measure of the electrostatic repulsive forces. Zeta potential is very important property as it provides information for the potential stability of colloidal nanoparticles. Unfortunately, there is no independent method to determine a zeta potential. The velocity of the charged particle is measured experimentally, from which the electrophoretic mobility is calculated, and then the zeta potential is calculated from the mobility. The correlation between the mobility and zeta potential depends on which theoretical model is used for the calculations. Two classic models are used for calculations, one being Huckel and the other Smoluchowski. Huckel approximation F(ka)=1.0 for ka<~1, and Smoluchowski approximation for F(ka)=1.5 for ka>~100, where k is reciprocal of 1/k which is the electric double layer thickness and a is the radii of the particle [18], [19]. From these two

models, Smoluchowski is typically used for colloids, and the following equation is applicable for calculating the zeta potential [20]:

$$\upsilon_E = 4\pi\varepsilon_o\varepsilon_r \frac{\zeta}{6\pi\eta}(1 + kr)$$

Where:

$\upsilon_E$ – Electrophoretic mobility

$\varepsilon_o$ – Relative dielectric constant

$\varepsilon_r$ – Electrical permittivity of a vacuum

$\zeta$ – Zeta potential

$\eta$ – Solution viscosity

k – Debye-Huckel parameter

r – Particle radius

The zeta potential value dictates the stability of the system. The absolute zeta potential values greater than 30 mV are generally taken as moderate or good stability dispersions. However, this definition can be sample dependent. Since zeta potential is dictated by the pH of the dispersions, determining the zeta potential of a dispersions at a range of pH's, is used to predict the behavior of colloids. Here, the isoelectric point (IEP) is the pH value at which the zeta potential is zero indicating that there is no surface charge on the particles. Such system exhibits poor stability. Table 1.2.1 summarizes typical zeta potential values corresponding to a stability behavior of colloids [21].

**Table 1.2.1 – Stability behavior of colloidal particles at different zeta potentials**

| Zeta potential, mV | Stability behavior of particles |
|---|---|
| 0 to $\pm$5 | Rapid coagulation or flocculation |
| ±10 to ±30 | Incipient instability |
| ±30 to ±40 | Moderate stability |
| ±40 to ± 60 | Good stability |
| More than ±61 | Excellent stability |

Derjaguin, Landau, Verwey, and Overbeek developed the DLVO theory which discusses the stability of colloids in terms of van der Waals repulsions and electrostatic double layer repulsions. Many researchers consider the DLVO theory to be a definite theory of electrostatic stabilization [22]. Based on the DLVO theory, the stability of colloids is dependent on the dominance of van der Waals attraction forces or the electric repulsive forces as particles approach one another as a result of Brownian motion. If the van der Waals forces overpower the repulsive forces, then the nanoparticles coagulate. This is known as a primary minimum. When the electric double layer repulsion forces overpower the van der Waals attractive forces, then the colloid exhibits the stability and is at a maximum energy barrier state. However, if the maximum energy barrier is high and cannot be overcome by the repulsive forces, then the particles end up being in a non-stable state. However, in this case these particles do not coagulate and can be redispersed easily. This condition is known as a secondary minimum [22]–[24]. The following equation sums up the DLVO theory:

$$V_T = V_R + V_A$$

Where:

$V_T$ – Total potential energy

$V_R$ – Repulsive potential energy

$V_A$ – Attractive potential energy

Figure 1.2.2 provides a schematic representation of the DLVO theory.

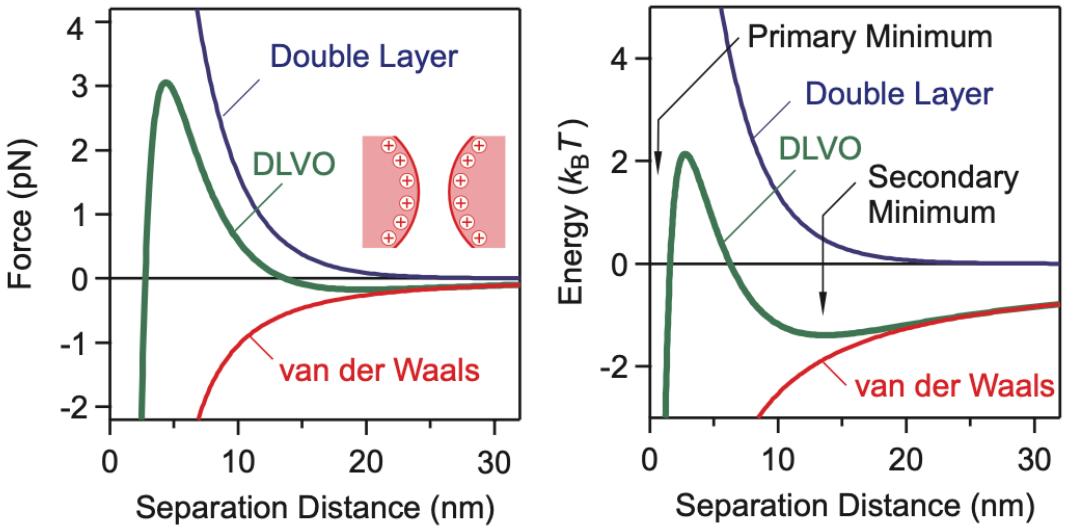


**Figure 1.2.2 – DLVO Theory** [24]

Figure 1.2.3 provides a schematic representation of various instability processes that are explained by DLVO theory.

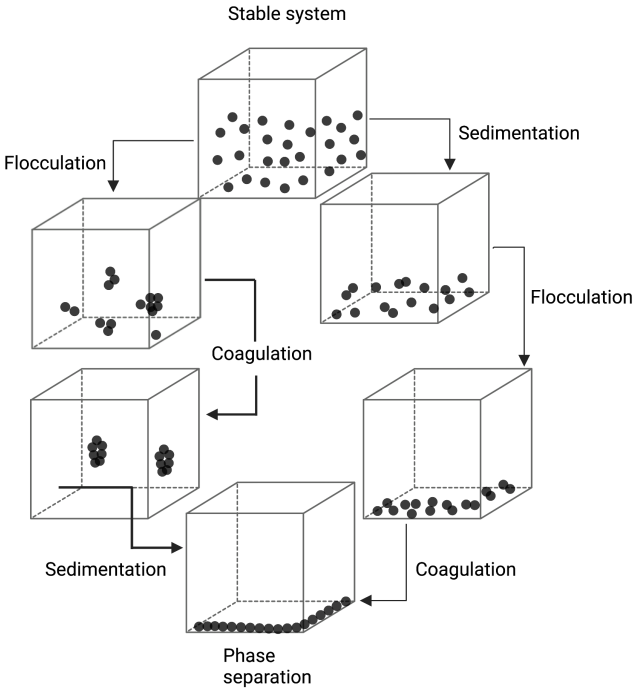


**Figure 1.2.3 – Colloids degradation mechanisms**[23]

Besides steric and electrostatic stabilization of colloidal systems, there is also a combination of steric and electrostatic stabilization which is known as electrosteric stabilization.

Particle size and polydispersity (or just dispersity per IUPAC recommendations) – the degree of non-uniformity [25], are two other parameters that are important in colloidal nanodispersion. Controlling the particle size and polydispersity is fundamental part of keeping dispersions stable during the established shelf life. Typically, the method of choice for measuring particles size of nanomaterials that have a spherical shape is dynamic light scattering (DLS). The DLS, also known as quasi-elastic light scattering (QELS) or photon correlation spectroscopy (PCS), is a technique which measures the changes in the intensity of light scattered from the dispersion to provide an information on the hydrodynamic diameter. The particle size is calculated using the Stokes Einstein equation:

$$D_h = \frac{k_B T}{3\pi\eta D_t}$$

Where:

$D_h$ – hydrodynamic diameter (particle size)

$D_t$ – Translational diffusion coefficient

$k_B$ – Boltzmann's constant

T – Thermodynamic temperature

η – Dynamic viscosity

From the equation is apparent that the temperature of the sample during the testing is important, also considering that viscosity is temperature dependent [26].

Polydispersity or polydispersity index (PDI) in DLS test is calculated from the following formula:

$$PDI = \left(\frac{Standard\ deviation}{Mean}\right)^2$$

Where:

S – standard deviation

M – mean

According to Malvenrn Panalytical, the PDI can be monodispersed if the value is less than 0.1, or polydispersed for values greater than 0.1. Furthermore, the monodispersed systems can be uniform when the PDI is 0, and narrow when PDI is between 0 and 0.1. For polydispersed systems, a value of 0.1-0.4 indicates a moderate dispersity, and a value >0.4 indicates a broad polydispersity [27].

To reduce the polydispersity the type and intensity of mechanical energy used, and the duration of the dispersion process are investigated in various systems. Mahbubul reported on the effect of duration of ultrasonication at 50% amplitude on the PDI of nanofluids [28]. It was reported that as the duration of the sonication increased, the PDI decreased. For the specific system and the experiment, the PDI was reduced from 0.34 without sonication to 0.24 after 2 hours of sonication [29]. In another study by Sadhegi et al, it was concluded that the PDI for $Al_2O_3$ dispersion decreased as the sonication time increased. After 30 minutes of sonication, the PDI was reported at 0.3 and decreased to 0.15 after 180 minutes of sonication. Additionally, the zeta potential increased and the particle size decreased as the sonication time was increased [30].

### 1.3 Titanium dioxide ($TiO_2$)

Titanium dioxide also known as titanium (IV) oxide or titania is a polymorph that exhibits three crystal structures: rutile, anatase and brookite. Rutile and anatase titanium dioxide have tetragonal unit cell structure. However, rutile has two $TiO_2$ units per unit cell, while the anatase

has four. The brookite has orthorhombic unit cell structure with eight $TiO_2$ units per unit cell. Figure 1.2.1 reports on the primitive cells of rutile, anatase and brookite.

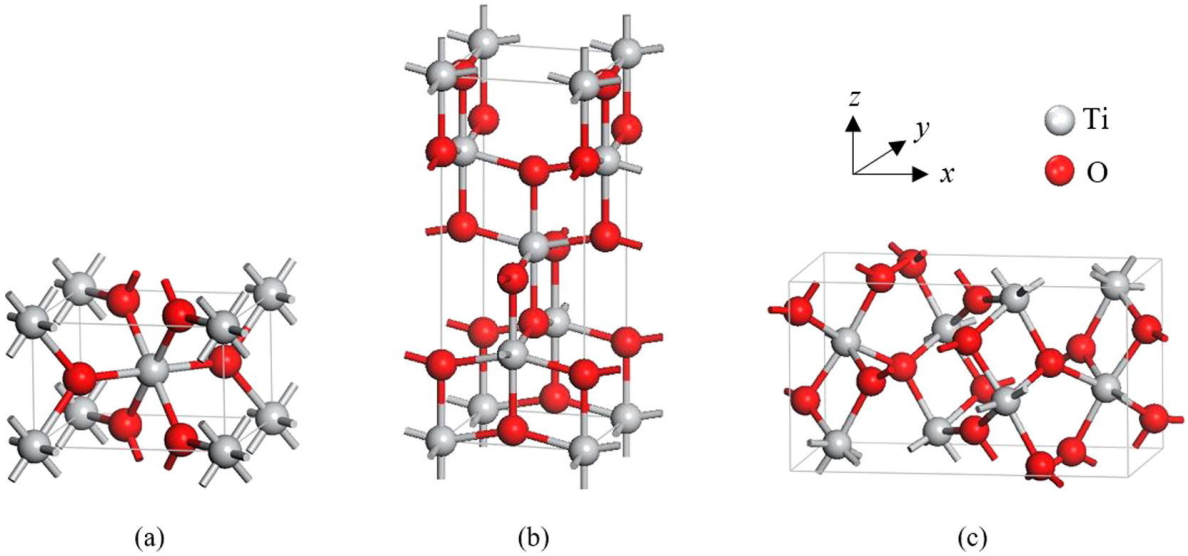


**Figure 1.3.1 – The primitive unit cell of (a) rutile, (b) anatase and (c) brookite** [31]

Figure 1.3.2 provides the x-ray diffractogram and Raman spectra for rutile, anatase and brookite.

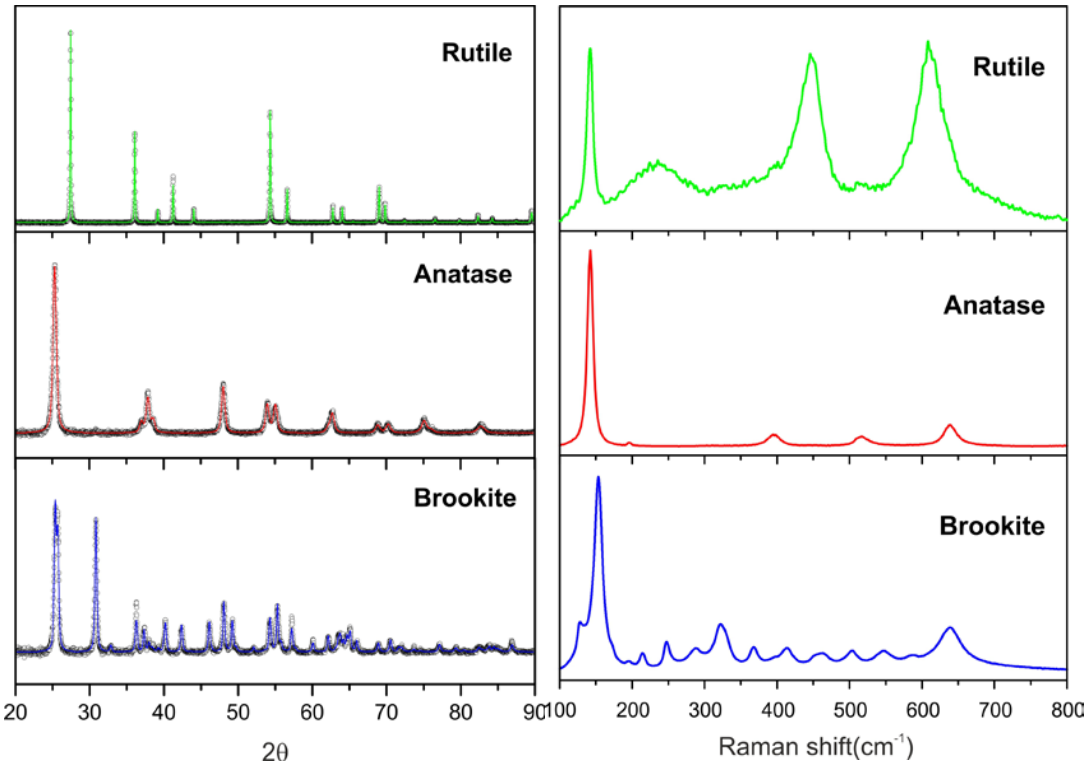


**Figure 1.3.2 - XRD patterns and Rietveld analysis of rutile, anatase and brookite (a) Corresponding Raman spectra (b)** [32]

From the three crystal structures, rutile and anatase are of higher importance for industry applications. These products were extensively used and researched in various fields, such as medical and pharmaceutical, food and cosmetic industry, as well as environmental applications. Even though interest has increased for studying brookite crystal structure, it is not as commonly utilized due to its complex structure and difficulty to be synthesized in its pure form [31].

One of many properties that titanium dioxide has is its ability to convert solar energy into chemical transformations, and further use this process to decompose organic matter, including bacteria and decompose inorganic pollutants such as nitric oxide ($NO_x$) and sulfuric oxide ($SO_x$) to their non-toxic salts. This process is known as photocatalysis. Additionally, superhydrophilicity is another important feature of titanium dioxide that gives its superior self-cleaning properties. As a result of its strong oxidizing properties, antimicrobial decomposition,

superhydrophilicity, chemical stability and relatively low cost, titanium dioxide is one of the most used and researched semiconductor photocatalyst [33]. When comparing the rutile and anatase, the anatase crystal structure has higher photocatalytic activity than the rutile. Anatase $TiO_2$ has a bandgap of 3.2 eV, while rutile $TiO_2$ has a band gap of 3.0 eV. It is well researched that anatase crystallite has a higher photocatalytic activity than rutile [33]. However, often a mixture of two polymorphs, anatase and rutile is used. For example, Aeroxide $TiO_2$ P 25 (formerly Degussa $TiO_2$ P 25) is a mixture of anatase with rutile crystallite due to the synergistic effect that leads to enhanced photocatalytic activity [34].

Titanium dioxide nanoparticles (NP) find a wide use for photocatalysis due to their small particle size and large surface area. Here, the particle size, surface area and surface chemistry play a significant role in creating stable nanoparticle dispersions in aqueous media. Therefore, to optimize the full potential of titanium dioxide nanoparticles and develop stable dispersions, as required for safe application in the field, it is highly important to understand the interactions at the solid-liquid level between the $TiO_2$ particles and the aqueous media.

It is common practice to use ionic surfactants to stabilized titanium dioxide nanoparticle dispersions in aqueous systems. Here, the ionic surfactant can electrostatically stabilize the dispersion. It is important to note that by increasing the concentration of surfactants, the zeta potential increases, but the thickness of the double layer surrounding the surface of particles decreases. If the concentration of the surfactant is too high, then the double layer can be depleted, and the particles start to agglomerate. Many researchers had explored various ionic surfactant types to evaluate the stability of the titanium dioxide dispersions in water.

For example, Tsai et al studied the effect of sodium hexametaphosphate (SHMP) and polyacrylic acid (PAA) on the dispersions of $TiO_2$ (P25) nanopowders in de-ionic water using

the ultrasonic horn. From this study it was concluded that SHMP was a better surfactant than PAA as it yielded dispersions with smaller particle size and greater zeta potential. [33] In another study, Tkachenko et al studied the influence of nonionic Triton X-100 and anionic Atlas G-3300 surfactants on the particle size and zeta potential of titanium dioxide aqueous dispersions. It was concluded that the Atlas G-3300 was more effective than the Triton X-100. [34] In a study by Othman et al, PAA ($M_w$=2,000 g/mol) and ammonium polymethacrylate (Darvan C) were used to stabilize the titanium dioxide nanoparticles. The data indicated that PAA at 3 wt.% provided a better stability [35].

Nanosized titanium dioxide is one of the most researched and used photocatalyst today with Aeroxide $TiO_2$ P 25 being used as a benchmark material over the past decades. Therefore, there are many studies where different surfactants were tested among different fields. However, it is rather difficult to compare these results as the conditions the testing, testing equipment and procedures were different from study to study.

It is well known that ultrasonication is an effective way to disperse powder nanoparticles into aqueous media. However, it is imperative to mention that the sonication time and operation mode play an important role as the total amount of energy given to the system depends on the power and the duration of time. Furthermore, another important feature that needs to be considered is controlling the temperature during the sonication as a significant amount of heat is generated that can lead to volume loss, especially for smaller samples. High temperature that is generated can also affect the agglomeration and aggregation of different systems as the viscosity of the system is temperature dependent. Also, the concentration and volume of the samples prepared is important to be kept consistent for proper comparison to be made. The geometry and size of the sonic probe is important as the acoustic energy given to the system depends on the

shape and diameter of the probe, and its immersion depth into the sample. All these features are imperative when it comes to the dispersions of nanoparticles.

# 2. Materials and Methods

## 2.1 Materials used in the experiment

Evonik Aeroxide $TiO_2$ P 25 – Titanium dioxide

Aeroxide $TiO_2$ P 25 (CAS Number 13463-67-7) is hydrophilic fumed, white solid, free-floating nanopowder with 21 nm primary particle size (TEM), specific surface area (BET) of 35-65 $m^2/g$, tapped density of 130 g/l, sieve residue (Mocler, 45 μm) of ≤0.05 wt. %. It has a chemical composition of ≥99.50 % (by wt.) $TiO_2$, ≤0.300 % (by wt.) $Al_2O_3$, ≤0.200 % (by wt.) $SiO_2$, ≤0.010 % (by wt.) $Fe_2O_3$, and ≤0.300% (by wt.) HCl, according to the manufacturer product data sheet. The material is a unique combination of anatase and rutile crystals, with predominantly anatase but the exact composition is not disclosed by the manufacturer. According to Tobaldi et al. Aeroxide $TiO_2$ P 25 is composed of 76.3 wt. % anatase, 10.6 wt. % rutile and 13.0 wt.% amorphous phase using quantitative phase analysis (QPA) and advanced X-ray diffraction (XRD) methods such as Rietveld RIR and whole powder pattern modeling (WPPM) [36].

Figures 2.1.1, 2.1.2, 2.1.3 and 2.1.4 represent image under scanning electron microscope (SEM), X-ray diffractogram, Raman spectrum and BET surface area plot respectfully, of the Aeroxide $TiO_2$ P 25 material used in this study.

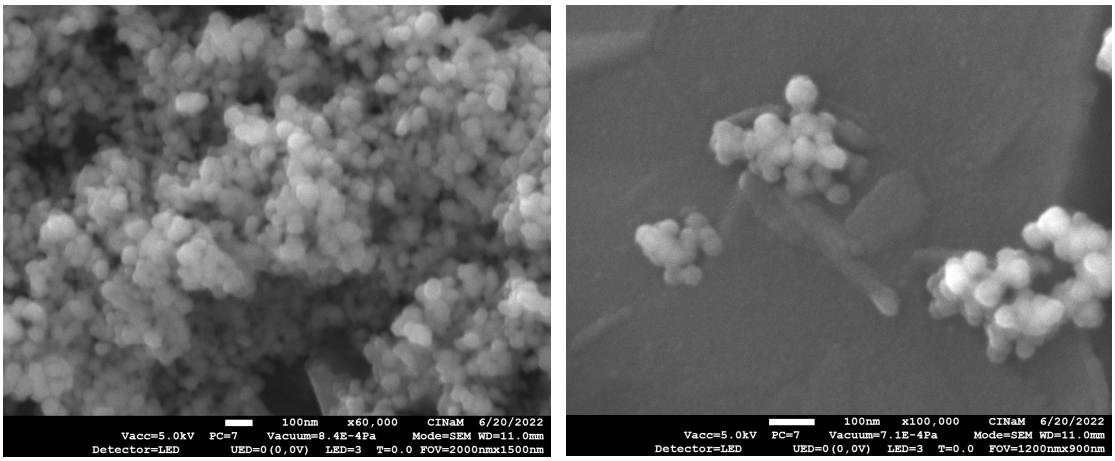


**Figure 2.1.1 – SEM image of Aeroxide P 25 with x60,000 magnification (left) and dispersed particles at x100,000 magnification (right)**

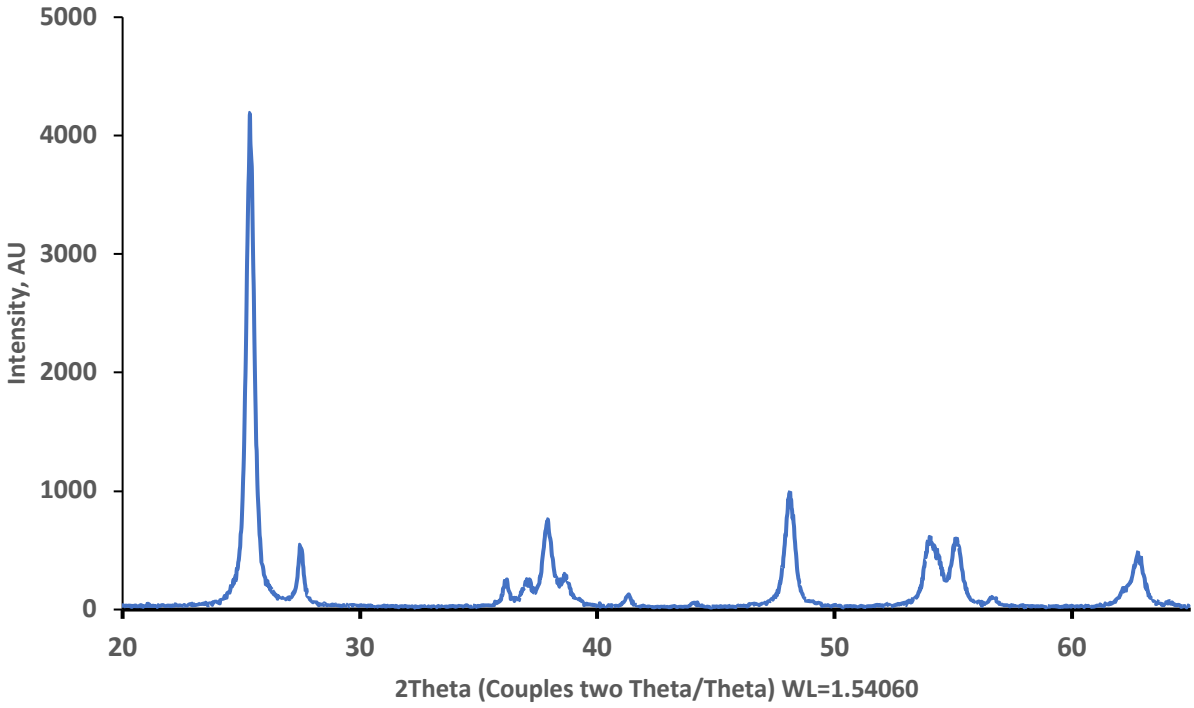


**Figure 2.1.2 X-ray diffractogram of Aeroxide $TiO_2$ P 25**

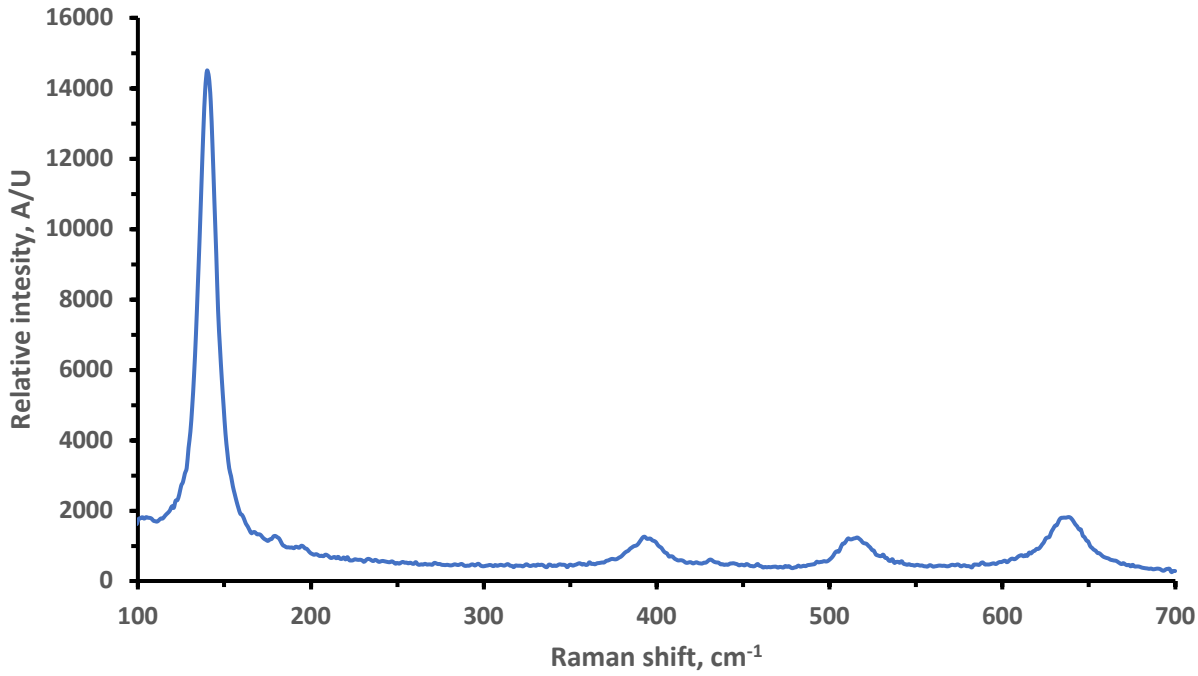


**Figure 2.1.3 Raman spectrum of Aeroxide $TiO_2$ P 25**

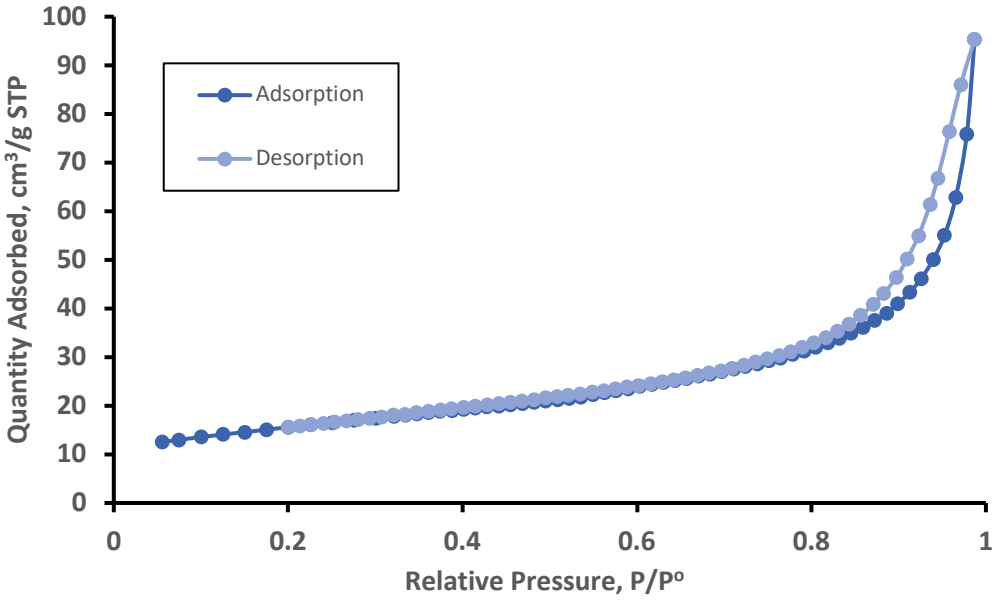


**Figure 2.1.4 BET isotherm plot of Aeroxide $TiO_2$ P 25**

Dow Tamol 731 DP – Hydrophobic copolymer dispersant

Tamol 731 DP is pale yellow to white powder, with solid content of 93 wt.% and density of 0.650 g/ml. It is an anionic surfactant which is the sodium salt of a carboxylate polyelectrolyte that has a high efficiency in dispersing inorganic pigments leading to good stability and is known to be compatible with a wide array of coating systems and rheology modifiers.

Figure 2.4 reports the FT-IR spectrum of the Tamol 731 DP material used in this study.

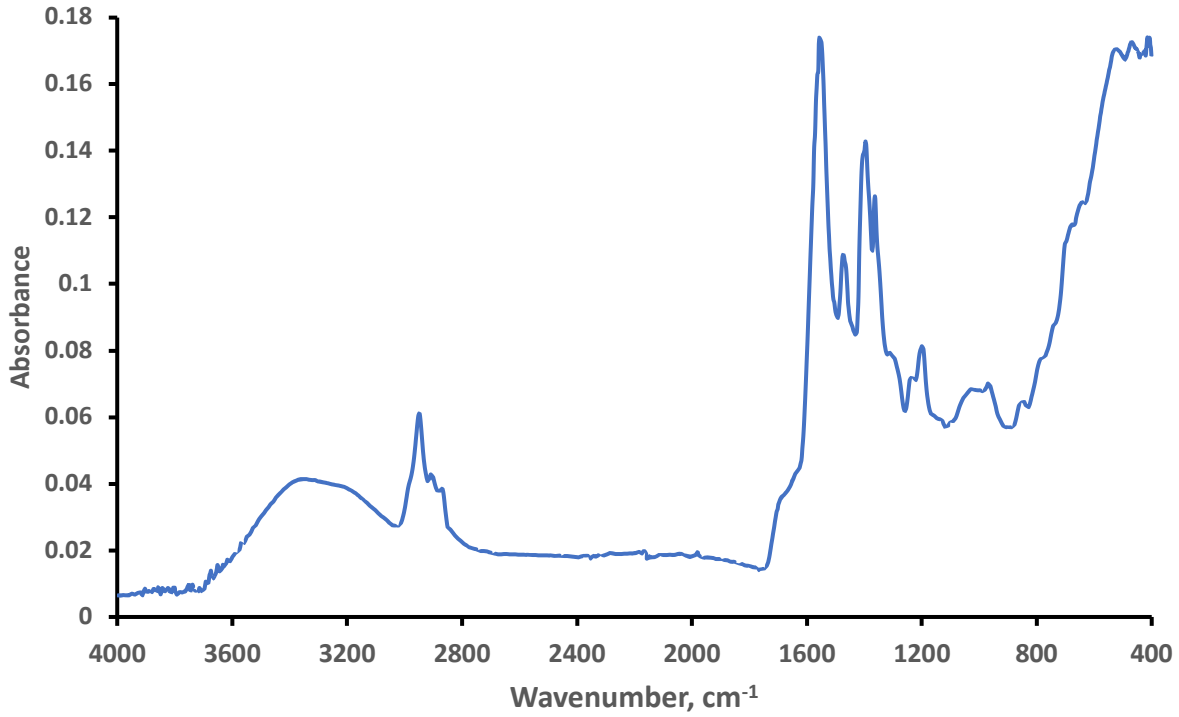


**Figure 2.1.5 FT-IR ATR of Tamol 731 DP**

BASF Dispex CX 4910

Dispex CX 4910 is a white powder, with solid content of 92 wt.% and density of 1.04 g/ml according to the manufacturer. It is an anionic surfactant which is the sodium salt of acrylic polymer and is highly effective dispersing agent tunned for application such as plaster, cement, and tile adhesive.

Figure 2.5 reports the FT-IR spectrum of the Dispex CX 4910 material used in this study.

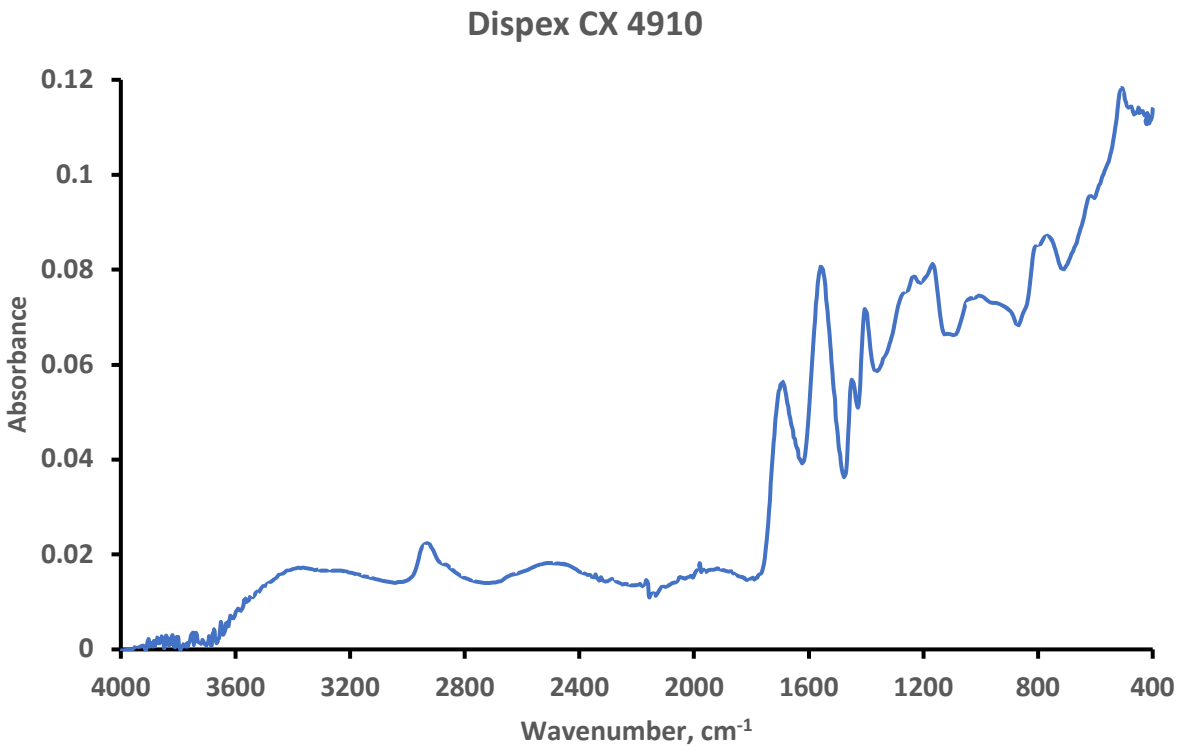


**Figure 2.1.6 FT-IR ATR of Dispex CX 4910**

18.2 MΩ water

De-ionic water (18.2 MΩ) from the University of Wisconsin-Milwaukee was used.

## 2.2 Equipment and experimental methods

### 2.2.1 Raw materials characterization

X-ray Diffraction (XRD)

Bruker X-ray diffraction unit was used to confirm the chemical composition and crystal structure of the Aeroxide $TiO_2$ P 25 material. The XRD patterns were obtained with 2θin the range of 20°-65° and WL=1.54060.

Raman Spectroscopy

Raman of Aeroxide $TiO_2$ P 25 spectrum was taken using Reinshaw 1000B 1800 grating HeNe (632.8nm – 35 mW) in a wavenumber from 100 $cm^{-1}$ – 700 $cm^{-1}$, for 10 seconds, extended, 20 objective and 10% power. The powder sample was stored at room temperature and was used for the testing.

Brunauer-Emmett-Teller (BET) Surface Area

Mi Micrometrics ASAP 2020 Surface Area and Porosity Analyzer was used to analyze the surface area, absorption, and desorption of the Aeroxide $TiO_2$ P 25 material.

Fourier Transform-Infrared Spectroscopy (FT-IR)

The IR spectra of Tamol 731 DP and Dispex CX 4910 were obtained on a Perkin-Elmer Spectrum 3 FT-IR spectrometer in a wavenumbere range from 400 $cm^{-1}$ – 4000 $cm^{-1}$, and scans of 32 times. The samples were in a powder form and were stored at room temperature.

2.2.2 Dispersions experimental methods and equipment

Dynamic light scattering (DLS) Particle Analysis and Polydispersity

Dynamic light scattering (DLS) is also known as photon correlation spectroscopy or quasi elastic light scattering (QELS). It is technique used to determine the particle size and particle size distribution at the submicron level. Brookhaven Instruments Corporation (BIC) ZetaPALS Particle Sizing Software Ver. 4.16 was used to obtain the particle size and polydispersity.

Approximately ¾ of volume (2 ml) of 18.2 MΩ DI water was added into a disposable 1 cm square, acrylic cuvette. A drop of a sample was added into the cuvette for each run, and the sample was gently mixed which resulted in a slight turbidity. The cuvette was then placed in the holder of

the instrument for analysis. All samples were run at 25 °C. Ten runs were used to obtain the mean effective diameter and polydispersity index.

Zeta (ζ) Potential

When particles are dispersed in liquid media, they often carry a charge on the surface. When subjected to an electric field, they will move either to the positive or negative pole, which is an indication of the charge they carry. The magnitude of the charge on the particles is proportional to the velocity they translate. From these results, using the Smoluchowsky equation, the zeta potential was calculated. In this study, Brookhaven Instruments Corporation (BIC) PALS Zeta Potential Analyzer Ver. 3.57 was used to obtain the zeta potential.

For this experiment a small amount of the sample was dispersed in 0.1 mM $KNO_3$ which resulted in a slightly turbid appearance. Approximately 1.5 ml of each sample was then placed in a disposable 1 cm square, acrylic cell and the electrode was inserted catching any spillages. The electrode was then connected to the lead and the cuvette was placed in the holder. Since the aqueous media was used to disperse the samples, Smoluchowsky method was used for the calculation. All samples were run at 23 °C. Five runs of seven cycles were used to obtain the mean value for the ζ potential.

pH

ASTM E70 Standard Test Method for pH of Aqueous Solutions with the Glass Electrode was used to measure the pH of the samples. Jenway 3520 Digital pH meter with glass electrode was used for testing the pH of all samples. It has pH range of -2 – 20 with pH accuracy of ±0.003, temperature range of -2 – 110 ̊C with temperature accuracy of ±0.5 ̊C and supports up to three-point calibration with manual or automatic buffer recognition.

A three-point calibration was performed to standardize the equipment before measuring the pH of the samples. The samples were agitated during measuring of the pH, and all tests were performed at a temperature of 22±2 ̊C.

Density

To measure the density of the samples, ASTM D1475 Standard Test Method for Liquid Coatings, Inks and Related Products was used. Gardco standard weight-per-gallon cup with accuracy of ±0.5% was used to measure the density of the samples.

First the volume of the container in ml, V was determined:

$$V = \frac{N-M}{\rho},$$

Where:

V – Volume of container, mL

N – weight of container and water, g

M – Weight of dry container, g

$\rho$ – Absolute density of water at specific temperature, g/ml

Furthermore, to calculate the density in g/ml, the following equation was used:

$$D_m = \frac{W - w}{V}$$

Where:

$D_m$ – Density, g/ml

W – Weight of filled container, g

W – weight of empty container, g

All samples were tested at temperature of 22±2 ̊C

## 2.3 Equipment used for preparation of samples

Silverson L5M-A Homognizer

Silverson L5M-A homogenizer was used to wet out and disperse the Aeroxide $TiO_2$ P 25 nanoparticles.

Propeller mixer

Mixer with propeller blade was used to wet out and disperse the Aeroxide $TiO_2$ P 25 nanoparticles. The diameter of the propeller blade used was at least 1/3 of the diameter of the container where the nanoparticles were wet out and dispersed.

Hielscher UIP1000hd ultrasonic Technology

Ultrasonic waves were used to deagglomerate the Aeroxide $TiO_2$ P 25 nanoparticles. A ultrasonic probe with a 2.5 cm diameter was used.

Fisher Scientific ultrasonic bath, model 15337410

Samples were stored at an ultrasonic bath between the ultrasonication for conditioning and stabilization purposes.

# 3. Experimental Design

## 3.1 Objective

The main objective of this study was to develop stable dispersions of titanium dioxide that can further be utilized in coatings, treatments, and components of cement-based materials. Stability, as defined in this program of study, was visually evaluated to ensure that no separation of the particles such as sedimentation was observed, or significant increase in particle size (effective diameter) and polydispersity, occurred over time. Two different concertations of titanium dioxide were used to compare whether the concentration played a role in the stability and particle size. The dispersions were made with and without anionic surfactants (electrostatically stabilized). Two different anionic surfactants were used, each at two different concentrations. Table 3.1 summarizes the theoretical composition of all formulae used.

**Table 3.1 Theoretical formula matrix in wt.%**

| Formula ID | 18.2 MΩ water, wt.% | Aeroxide $TiO_2$ P 25, wt.% | 0.1% Tamol 731 DP in 18.2 MΩ water, wt.% | 0.2% Tamol 731 DP in 18.2 MΩ water, wt.% | 0.1% Dispex CX 4910 in 18.2 MΩ water, wt.% | 0.2% Dispex CX 4910 in 18.2 MΩ water, wt.% |
|---|---|---|---|---|---|---|
| C-F-1-N | 99.0000 | 1.0000 | | | | |
| F-1-N | 99.0000 | 1.0000 | | | | |
| F-1-N(2) | 99.0000 | 1.0000 | | | | |
| F-2-N | 98.0000 | 2.0000 | | | | |
| F-1-A-1 | | 1.0000 | 99.0000 | | | |
| F-2-A-1 | | 2.0000 | 98.0000 | | | |
| F-1-A-2 | | 1.0000 | | 99.0000 | | |
| F-2-A-2 | | 2.0000 | | 98.0000 | | |
| F-1-B-1 | | 1.0000 | | | 99.0000 | |
| F-2-B-1 | | 2.0000 | | | 98.0000 | |
| F-1-B-2 | | 1.0000 | | | | 99.0000 |
| F-2-B-2 | | 2.0000 | | | | 98.0000 |

The following formula identification was used:

$$C - F - \frac{1}{2} - \frac{A}{\frac{B}{N}} - \frac{1}{\frac{2}{(2)}}$$

Where:

| | |
|---|---|
| C-F | Homogenization or mixing was used for making the samples; |
| F | Combined homogenization or mixing and ultrasonic processing were used for sample preparation; |
| 1 or 2 | Number following the letter "F" refers to the amount of $TiO_2$ used (1 for 1 wt.% and 2 for 2 wt.%); |
| A or B or N | Indicates if a surfactant was used and which type (A for Tamol 731 DP, B for Dispex CX 4910, and N for no surfactant); |
| 1 or 2 | Number following the letter "A or B" indicates the level of surfactant used (1 for 0.1 wt.% and 2 for 0.2 wt.%); |
| (2) | (2) following the letter "N" indicates that this is a replica sample of an existing formula that used different type of mechanical energy for wetting out the nanoparticles |

## 3.2 Experimental Matrix

Twelve different formulations were made, each in replicates of three. All formulations were produced using Aeoroxide $TiO_2$ P25 nanoparticles that were first wetted out in 18.2 MΩ water or an anionic surfactant solution using propeller blade mixer or Silverson LM5-A homogenizer for ten minutes. All the water (with surfactant when specified) was added first, the mixer or homogenizer was turned on, and the nanopowder was added slowly over period of two minutes.

The dispersions were mixed or homogenized for additional eight minutes, so the total agitated mixing was for 10 minutes.

To evaluate whether this approach was sufficient to create a stable dispersion, C-F-1-A formula was made in replicate of three, using Silverson M-5 homogenizer. Another formula, F-1-A was made using the exact same method as for C-F-1-A, however, it was additionally sonicated for five minutes at 80% intensity. Then it was placed in a sonication bath for 30 minutes, following by another five minutes of sonication at 80% intensity, and finishing with additional 30 minutes in a sonic bath. Table 3.2.1 and 3.2.2 summarize the actual quantity of each ingredient used and the actual manufacturing procedure parameters used for formula C-F-1-A and F-1-A.

**Table 3.2.1 – Formula and manufacturing parameters for C-F-1-N**

| C-F-1-N | Theoretical quantity, wt.% | Actual quantity, wt.% | | |
|---|---|---|---|---|
| Ingredients | | Sample A | Sample B* | Sample C |
| 18.2 MΩ Water | 99.0000 | 99.0174 | 99.0079 | 99.0012 |
| Aeroxide $TiO_2$ P 25 | 1.0000 | 1.0006 | 1.0050 | 1.0089 |
| Step 1: Wetting out of $TiO_2$ P 25 using mechanical mixing (homogenization) | | | | |
| Total mix time (with homogenizer), minutes | 10 | 10 | 10 | 10 |
| Beginning Speed, rpm | Report | 3100 | 3070 | 3060 |
| End Speed, rpm | Report | 4010 | 4090 | 4060 |
| Temperature after homogenizing, ˚C | Report | 35.3 | 29.2 | 33.2 |

*This sample was cross-contaminated

**Table 3.2.2 – Formula and manufacturing parameters for F-1-N**

| F-1-N | Theoretical quantity, wt.% | Actual quantity, wt.% | | |
|---|---|---|---|---|
| Ingredients | | Sample A | Sample B | Sample C |
| 18.2 MΩ Water | 99.0000 | 99.0337 | 99.0039 | 99.0373 |
| Aeroxide $TiO_2$ P 25 | 1.0000 | 1.0009 | 1.0017 | 1.023 |
| Step 1: Wetting out of $TiO_2$ P 25 using mechanical mixing (homogenization) | | | | |
| Total mix time (with homogenizer), minutes: | 10 | 10 | 10 | 10 |
| Beginning Speed, rpm: | Report | 3070 | 3080 | 3080 |
| End Speed, rpm: | Report | 3770 | 3840 | 3820 |
| Temperature after homogenizing, ˚C: | Report | 30 | 29.2 | 31.3 |
| Step 2: Ultrasonication | | | | |
| 1st ultrasonication at 80% intensity, %: | 5 | 5 | 5 | 5 |
| Temperature after 1st ultrasonication ˚C: | Report | 52.3 | 53.3 | 50.9 |
| 1st ultrasonic bath conditioning, minutes: | 30 | 30 | 30 | 30 |
| Temperature after 1st ultrasonic bath conditioning, ˚C: | Report | 29.2 | 37.3 | 35.3 |
| 2nd ultrasonication at 80% intensity, %: | 5 | 5 | 5 | 5 |
| Temperature after 2nd ultrasonication, ˚C: | Report | 47.3 | 53.6 | 50.8 |
| 2nd ultrasonic bath conditioning, minutes: | 30 | 30 | 30 | 30 |
| Temperature after 2nd ultrasonic bath conditioning, ˚C: | Report | 37.3 | 32.4 | 36.3 |

The F-1-N(2) was the same formula as F-1-N, however, a propeller blade mixer instead of a homogenizer was used to wet-out the titanium dioxide nanoparticles, prior to ultrasonication.

Table 3.2.3 summarized the actual quantity of each ingredient used and the actual manufacturing procedure parameters.

**Table 3.2.3 – Formula and manufacturing parameters for F-1-N(2)**

| F-1-N(2) | Theoretical quantity, wt.% | Actual quantity, wt.% | | |
|---|---|---|---|---|
| Ingredients | | Sample A | Sample B | Sample C |
| 18.2 MΩ Water | 99.0000 | 99.009 | 99.0202 | 99.018 |
| Aeroxide $TiO_2$ P 25 | 1.0000 | 1.0077 | 1.0043 | 1.0028 |
| Step 1: Wetting out of $TiO_2$ P 25 using mechanical mixing (mixing with propeller blade) | | | | |
| Total mix time (with propeller mixer) minutes: | 10 | 10 | 10 | 10 |
| Beginning Speed, level: | Report | 1 | 1 | 1 |
| End Speed, level: | Report | 1 | 1 | 1 |
| Temperature after mixing, ˚C: | Report | 21.9 | 21.6 | 20.9 |
| Step 2: Ultrasonication | | | | |
| 1st ultrasonication at 80% intensity, %: | 5 | 5 | 5 | 5 |
| Temperature after 1st ultrasonication ˚C: | Report | 51.3 | 54.7 | 52.2 |
| 1st ultrasonic bath conditioning, minutes: | 30 | 30 | 30 | 30 |
| Temperature after 1st ultrasonic bath conditioning, ˚C: | Report | 35.7 | 39.2 | 38.6 |
| 2nd ultrasonication at 80% intensity, %: | 5 | 5 | 5 | 5 |
| Temperature after 2nd ultrasonication, ˚C: | Report | 60.2 | 50.1 | 52.6 |
| 2nd ultrasonic bath conditioning, minutes: | 30 | 30 | 30 | 30 |
| Temperature after 2nd ultrasonic bath conditioning, ˚C: | Report | 41 | 41.6 | |

Tables 3.2.4 through 3.2.12 summarize the actual quantity of each ingredient used and the actual manufacturing procedure parameters in F-2-N, F-1-A-1, F-2-A-1, F-1-A-2, F-2-A-2, F-1-B-1, F-2-B-1, F-1-B-2, and F-2-B-2 compositions.

**Table 3.2.4 – Formula and manufacturing parameters for F-2-N**

| F-2-N | Theoretical quantity, wt.% | Actual quantity, wt.% | | |
|---|---|---|---|---|
| Ingredients | | Sample 1 | Sample 2 | Sample 3 |
| 18.2 MΩ Water | 98.0000 | 98.0112 | 98.0361 | 98.0149 |
| Aeroxide $TiO_2$ P 25 | 2.0000 | 2.0011 | 2.0005 | 2.0002 |
| Step 1: Wetting out of $TiO_2$ P 25 using mechanical mixing (homogenization) | | | | |
| Total mix time (with homogenizer), minutes: | 10 | 10 | 10 | 10 |
| Beginning Speed, rpm: | Report | 3120 | 3080 | 3080 |
| End Speed, rpm: | Report | 4070 | 4090 | 4020 |
| Temperature after homogenizing, ˚C: | Report | 35.2 | 33.2 | 34 |
| Step 2: Ultrasonication | | | | |
| 1st ultrasonication at 80% intensity, minutes: | 5 | 5 | 5 | 5 |
| Temperature after 1st ultrasonication ˚C: | Report | 52.1 | 48.6 | 50 |
| 1st ultrasonic bath conditioning, minutes: | 30 | 30 | 30 | 30 |
| Temperature after 1st ultrasonic bath conditioning, ˚C: | Report | 35.3 | 35.3 | 31.1 |
| 2nd ultrasonication at 80% intensity, minutes: | 5 | 5 | 5 | 5 |
| Temperature after 2nd ultrasonication, ˚C: | Report | 51.3 | 52.3 | 58.2 |
| 2nd ultrasonic bath conditioning, minutes: | 30 | 30 | 30 | 30 |
| Temperature after 2nd ultrasonic bath conditioning, ˚C: | Report | 39.4 | 30.1 | 35.3 |

**Table 3.2.5 – Formula and manufacturing parameters for F-1-A-1**

| F-1-A-1 | Theoretical quantity, wt.% | Actual quantity, wt.% | | |
|---|---|---|---|---|
| Ingredients | | Sample 1 | Sample 2 | Sample 3 |
| 0.1% Tamol 731 DP solution in 18.2 MΩ water | 99.0000 | 99.0336 | 99.0134 | 99.0302 |
| Aeroxide $TiO_2$ P 25 | 1.0000 | 1.0026 | 1.0043 | 1.001 |
| Step 1: Wetting out of $TiO_2$ P 25 using mechanical mixing (homogenization) | | | | |
| Total mix time (with homogenizer), minutes: | 10 | 10 | 10 | 10 |
| Beginning Speed, rpm: | Report | 3030 | 3080 | 3040 |
| End Speed, rpm: | Report | 4040 | 4070 | 4030 |
| Temperature after homogenizing, ˚C: | Report | 36.7 | 36.9 | 35.2 |
| Step 2: Ultrasonication | | | | |
| 1st ultrasonication at 80% intensity, minutes: | 5 | 5 | 5 | 5 |
| Temperature after 1st ultrasonication ˚C: | Report | 52.6 | 50.7 | 53.8 |
| 1st ultrasonic bath conditioning, minutes: | 30 | 30 | 30 | 30 |
| Temperature after 1st ultrasonic bath conditioning, ˚C: | Report | 35.3 | 36.3 | 36.8 |
| 2nd ultrasonication at 80% intensity, minutes: | 5 | 5 | 5 | 5 |
| Temperature after 2nd ultrasonication, ˚C: | Report | 53.6 | 52.6 | 53.3 |
| 2nd ultrasonic bath conditioning, minutes: | 30 | 30 | 30 | 30 |
| Temperature after 2nd ultrasonic bath conditioning, ˚C: | Report | 30 | 35.7 | 35.2 |

**Table 3.2.6 – Formula and manufacturing parameters for F-2-A-1**

| F-2-A-1 | Theoretical quantity, wt.% | Actual | | |
|---|---|---|---|---|
| Ingredients | | Sample 1 | Sample 2 | Sample 3 |
| 0.1% Tamol 731 DP solution in 18.2 MΩ water | 98.0000 | 98.0127 | 98.028 | 98.0055 |
| Aeroxide $TiO_2$ P 25 | 2.0000 | 2.0025 | 2.0042 | 2.0065 |
| Step 1: Wetting out of $TiO_2$ P 25 using mechanical mixing (homogenization) | | | | |
| Total mix time (with homogenizer), minutes: | 10 | 10 | 10 | 10 |
| Beginning Speed, rpm: | Report | 3040 | 3030 | 3040 |
| End Speed, rpm: | Report | 4020 | 4020 | 4020 |
| Temperature after homogenizing, ˚C: | Report | 35.5 | 31.8 | 36.3 |
| Step 2: Ultrasonication | | | | |
| 1st ultrasonication at 80% intensity, minutes: | 5 | 5 | 5 | 5 |
| Temperature after 1st ultrasonication ˚C: | Report | 51.3 | 55.3 | 61.8 |
| 1st ultrasonic bath conditioning, minutes: | 30 | 30 | 30 | 30 |
| Temperature after 1st ultrasonic bath conditioning, ˚C: | Report | 38.4 | 29.6 | 34.6 |
| 2nd ultrasonication at 80% intensity, minutes: | 5 | 5 | 5 | 5 |
| Temperature after 2nd ultrasonication, ˚C: | Report | 55.3 | 52.8 | 63.8 |
| 2nd ultrasonic bath conditioning, minutes: | 30 | 30 | 30 | 30 |
| Temperature after 2nd ultrasonic bath conditioning, ˚C: | Report | 34.9 | 31.1 | |

**Table 3.2.7 – Formula and manufacturing parameters for F-1-A-2**

| F-1-A-2 | Theoretical | Actual | | |
|---|---|---|---|---|
| Ingredients | Qty, % | Sample 1 | Sample 2 | Sample 3 |
| 0.2% Tamol 731 DP solution in 18.2 MΩ water | 99.0000 | 99.0151 | 99.0018 | 99.0357 |
| Aeroxide $TiO_2$ P 25 | 1.0000 | 1.0014 | 1 | 1.0089 |
| Step 1: Wetting out of $TiO_2$ P 25 using mechanical mixing (homogenization) | | | | |
| Total mix time (with homogenizer), minutes: | 10 | 10 | 10 | 10 |
| Beginning Speed, rpm: | Report | 3100 | 3050 | 3100 |
| End Speed, rpm: | Report | 4080 | 4080 | 4120 |
| Temperature after homogenizing, ˚C: | Report | 34.7 | 36.7 | 32.6 |
| Step 2: Ultrasonication | | | | |
| 1st ultrasonication at 80% intensity, minutes: | 5 | 5 | 5 | 5 |
| Temperature after 1st ultrasonication ˚C: | Report | 53.3 | 56.3 | 53 |
| 1st ultrasonic bath conditioning, minutes: | 30 | 30 | 30 | 30 |
| Temperature after 1st ultrasonic bath conditioning, ˚C: | Report | 30.1 | 33.1 | 33.5 |
| 2nd ultrasonication at 80% intensity, minutes: | 5 | 5 | 5 | 5 |
| Temperature after 2nd ultrasonication, ˚C: | Report | 50.3 | 53.7 | 56.2 |
| 2nd ultrasonic bath conditioning, minutes: | 30 | 30 | 30 | 30 |
| Temperature after 2nd ultrasonic bath conditioning, ˚C: | Report | 33.7 | 38.6 | 40.6 |

**Table 3.2.8 – Formula and manufacturing parameters for F-2-A-2**

| F-2-A-2 | Theoretical quantity, wt.% | Actual quantity, wt.% | | |
|---|---|---|---|---|
| Ingredients | | Sample 1 | Sample 2 | Sample 3* |
| 0.2% Tamol 731 DP solution in 18.2 MΩ water | 98.0000 | 98.0045 | 98.02 | |
| Aeroxide $TiO_2$ P 25 | 2.0000 | 2.0098 | 2.0035 | |
| Step 1: Wetting out of $TiO_2$ P 25 using mechanical mixing (homogenization) | | | | |
| Total mix time (with homogenizer), minutes: | 10 | 10 | 10 | 10 |
| Beginning Speed, rpm: | Report | 3030 | 3030] | |
| End Speed, rpm: | Report | 4120 | 4010 | |
| Temperature after homogenizing, ˚C: | Report | 36.6 | 35.3 | |
| Step 2: Ultrasonication | | | | |
| 1st ultrasonication at 80% intensity, minutes: | 5 | 5 | 5 | 5 |
| Temperature after 1st ultrasonication ˚C: | Report | 59.8 | 51.9 | |
| 1st ultrasonic bath conditioning, minutes: | 30 | 30 | 30 | 30 |
| Temperature after 1st ultrasonic bath conditioning, ˚C: | Report | 36.1 | 39.6 | |
| 2nd ultrasonication at 80% intensity, minutes: | 5 | 5 | 5 | 5 |
| Temperature after 2nd ultrasonication, ˚C: | Report | 56 | 61.1 | |
| 2nd ultrasonic bath conditioning, minutes: | 30 | 30 | 30 | 30 |
| Temperature after 2nd ultrasonic bath conditioning, ˚C: | Report | 42.5 | 44.7 | |

**Table 3.2.9 – Formula and manufacturing parameters for F-1-B-1**

| F-1-B-1 | Theoretical | Actual | | |
|---|---|---|---|---|
| Ingredients | Qty, % | Sample A | Sample B | Sample C |
| 0.1% Dispex CX 4910 solution in 18.2 MΩ water | 99.0000 | 99.0305 | 99.0299 | 99.0765 |
| Aeroxide $TiO_2$ P 25 | 1.0000 | 1.0091 | 1.0096 | 1.0029 |
| Step 1: Wetting out of $TiO_2$ P 25 using mechanical mixing (propeller blade mixer) | | | | |
| Total mix time (with propeller blade mixer), minutes: | 10 | 10 | 10 | 10 |
| Beginning Speed, level: | Report | 1 | 1 | 1 |
| End Speed, level: | Report | 1 | 1 | 1 |
| Temperature after mixing, ˚C: | Report | 21.9 | 21.6 | 20.9 |
| Step 2: Ultrasonication | | | | |
| 1st ultrasonication at 80% intensity, minutes: | 5 | 5 | 5 | 5 |
| Temperature after 1st ultrasonication ˚C: | Report | 50 | 61.3 | 51.9 |
| 1st ultrasonic bath conditioning, minutes: | 30 | 30 | 30 | 30 |
| Temperature after 1st ultrasonic bath conditioning, ˚C: | Report | 33.2 | 36.3 | 40.2 |
| 2nd ultrasonication at 80% intensity, minutes: | 5 | 5 | 5 | 5 |
| Temperature after 2nd ultrasonication, ˚C: | Report | 55.8 | 52.9 | 55.6 |
| 2nd ultrasonic bath conditioning, minutes: | 30 | 30 | 30 | 30 |
| Temperature after 2nd ultrasonic bath conditioning, ˚C: | Report | 42.6 | 32.9 | 36.2 |

**Table 3.2.10 – Formula and manufacturing parameters for F-2-B-1**

| F-2-B-1 | Theoretical | Actual | | |
|---|---|---|---|---|
| Ingredients | Qty, % | Sample A | Sample B | Sample C |
| 0.1% Dispex CX 4910 solution in 18.2 MΩ water | 98.0000 | 98.0360 | 98.0205 | 98.0193 |
| Aeroxide $TiO_2$ P 25 | 2.0000 | 2.0095 | 2.0118 | 2.0149 |
| Step 1: Wetting out of $TiO_2$ P 25 using mechanical mixing (propeller blade mixer) | | | | |
| Total mix time (with propeller blade mixer), minutes: | 10 | 10 | 10 | 10 |
| Beginning Speed, level: | Report | 1 | 1 | 1 |
| End Speed, level: | Report | 1 | 1 | 1 |
| Temperature after mixing, ˚C: | Report | 22.6 | 21.6 | 21.5 |
| Step 2: Ultrasonication | | | | |
| 1st ultrasonication at 80% intensity, minutes: | 5 | 5 | 5 | 5 |
| Temperature after 1st ultrasonication ˚C: | Report | 44.4 | 51.7 | 46 |
| 1st ultrasonic bath conditioning, minutes: | 30 | 30 | 30 | 30 |
| Temperature after 1st ultrasonic bath conditioning, ˚C: | Report | 27.2 | 31.1 | 34.5 |
| 2nd ultrasonication at 80% intensity, minutes: | 5 | 5 | 5 | 5 |
| Temperature after 2nd ultrasonication, ˚C: | Report | 54 | 52.2 | 57.9 |
| 2nd ultrasonic bath conditioning, minutes: | 30 | 30 | 30 | 30 |
| Temperature after 2nd ultrasonic bath conditioning, ˚C: | Report | 36.9 | 25.9 | 28.3 |

**Table 3.2.11 – Formula and manufacturing parameters for F-1-B-2**

| F-1-B-2 | Theoretical | Actual | | |
|---|---|---|---|---|
| Ingredients | Qty, % | Sample A | Sample B | Sample C |
| 0.2% Dispex CX 4910 solution in 18.2 MΩ water | 99.0000 | 99.0017 | 99.0195 | 99.0193 |
| Aeroxide $TiO_2$ P 25 | 1.0000 | 1.0016 | 1.0082 | 1.0028 |
| Step 1: Wetting out of $TiO_2$ P 25 using mechanical mixing (propeller blade mixer) | | | | |
| Total mix time (with homogenizer), minutes: | 10 | 10 | 10 | 10 |
| Beginning Speed, level: | Report | 1 | 1 | 1 |
| End Speed, level: | Report | 1 | 1 | 1 |
| Temperature after mixing, ˚C: | Report | 21.1 | 20.8 | 21.0 |
| Step 2: Ultrasonication | | | | |
| 1st ultrasonication at 80% intensity, minutes: | 5 | 5 | 5 | 5 |
| Temperature after 1st ultrasonication ˚C: | Report | 53 | 52.9 | 55.9 |
| 1st ultrasonic bath conditioning, minutes: | 30 | 30 | 30 | 30 |
| Temperature after 1st ultrasonic bath conditioning, ˚C: | Report | 35.8 | 30.2 | 35.8 |
| 2nd ultrasonication at 80% intensity, minutes: | 5 | 5 | 5 | 5 |
| Temperature after 2nd ultrasonication, ˚C: | Report | 54.2 | 55.8 | 56.2 |
| 2nd ultrasonic bath conditioning, minutes: | 30 | 30 | 30 | 30 |
| Temperature after 2nd ultrasonic bath conditioning, ˚C: | Report | 38.6 | 40.6 | 40.8 |

**Table 3.2.11 – Formula and manufacturing parameters for F-2-B-2**

| F-2-B-2 | Theoretical quantity, wt.% | Actual quantity, wt. % | | |
|---|---|---|---|---|
| Ingredients | | Sample A | Sample B | Sample C |
| 0.2% Dispex CX 4910 solution in 18.2 MΩ water | 98.0000 | 98.0178 | 98.0186 | 98.0280 |
| Aeroxide $TiO_2$ P 25 | 2.0000 | 2.0030 | 2.0075 | 2.0041 |
| Step 1: Wetting out of $TiO_2$ P 25 using mechanical mixing (propeller blade mixer) | | | | |
| Total mix time (with propeller blade mixer), minutes: | 10 | 10 | 10 | 10 |
| Beginning Speed, level: | Report | 1 | 1 | 1 |
| End Speed, level: | Report | 1 | 1 | 1 |
| Temperature after mixing, ˚C: | Report | 22.1 | 21.6 | 21.6 |
| Step 2: Ultrasonication | | | | |
| 1st ultrasonication at 80% intensity, minutes: | 5 | 5 | 5 | 5 |
| Temperature after 1st ultrasonication ˚C: | Report | 51.1 | 55.8 | 53.6 |
| 1st ultrasonic bath conditioning, minutes: | 30 | 30 | 30 | 30 |
| Temperature after 1st ultrasonic bath conditioning, ˚C: | Report | 40.3 | 36.3 | 39.2 |
| 2nd ultrasonication at 80% intensity, minutes: | 5 | 5 | 5 | 5 |
| Temperature after 2nd ultrasonication, ˚C: | Report | 57.3 | 58.4 | 61.5 |
| 2nd ultrasonic bath conditioning, minutes: | 30 | 30 | 30 | 30 |
| Temperature after 2nd ultrasonic bath conditioning, ˚C: | Report | 27.5 | 30.5 | N/A |

## 4. Experimental Results and Discussion

### 4.1 Experimental Results

Test results for pH, density, zeta potential, particle size and polydispersity at 3±3 days, and particle size and polydispersity at 30±3 days are summarized in Table 4.1.1 through 4.1.15.

The pH values

Table 4.1.1 and Figure 4.1.1 summarize the data for the pH of all investigated samples when tested in accordance with ASTM E70.

**Table 4.1.1 – The pH values tested in accordance with ASTM E70**

| Formula | Sample A | Sample B | Sample C | Average | Standard deviation |
|---|---|---|---|---|---|
| C-F-1-N | 3.988 | 4.929 | 3.952 | 4.290 | 0.554 |
| F-1-N | 4.106 | 4.094 | 4.066 | 4.089 | 0.021 |
| F-1-N(2) | 3.978 | 4.025 | 3.984 | 3.996 | 0.026 |
| F-2-N | 4.039 | 3.977 | 3.984 | 4.000 | 0.034 |
| F-1-A-1 | 10.104 | 10.025 | 10.021 | 10.050 | 0.047 |
| F-2-A-1 | 9.269 | 9.222 | 9.209 | 9.233 | 0.032 |
| F-1-A-2 | 10.568 | 10.543 | 10.444 | 10.518 | 0.066 |
| F-2-A-2 | 9.905 | 9.852 | 9.764 | 9.840 | 0.071 |
| F-1-B-1 | 6.702 | 6.677 | 6.714 | 6.698 | 0.019 |
| F-2-B-1 | 6.773 | 6.792 | 6.797 | 6.787 | 0.013 |
| F-1-B-2 | 6.429 | 6.426 | 6.412 | 6.422 | 0.009 |
| F-2-B-2 | 6.574 | 6.536 | 6.481 | 6.530 | 0.047 |

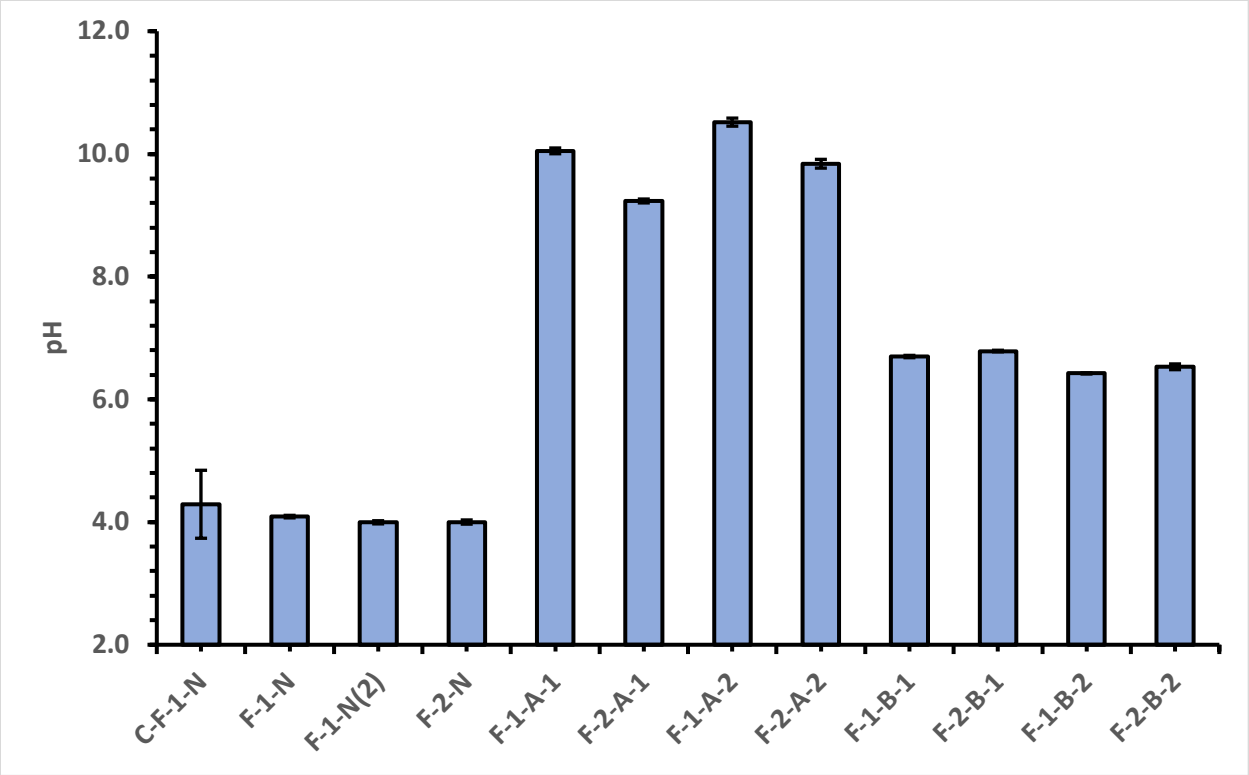


**Figure 4.1.1 – The pH values tested in accordance with ASTM E70**

Density

Table 4.1.2 and Figure 4.1.2 summarize the data for the density (reported in g/ml) of all samples when tested in accordance with ASTM D1475.

**Table 4.1.2 – Density tested in accordance with ASTM D1475 (g/ml)**

| Formula | Sample A | Sample B | Sample C | Average | Standard Deviation |
|---|---|---|---|---|---|
| C-F-1-N | 1.002 | 1.001023 | 1.003078 | 1.002 | 0.001043 |
| F-1-N | 1.003 | 1.002387 | 1.003458 | 1.003 | 0.000578 |
| F-1-N(2) | 1.001 | 1.001917 | 1.001797 | 1.002 | 0.00012 |
| F-2-N | 1.009 | 1.009467 | 1.009467 | 1.009 | 6.92E-05 |
| F-1-A-1 | 1.004 | 1.003602 | 1.003765 | 1.004 | 0.000111 |
| F-2-A-1 | 1.010 | 1.010306 | 1.010186 | 1.010 | 0.00012 |
| F-1-A-2 | 1.002 | 1.003827 | 1.003989 | 1.003 | 0.000955 |
| F-2-A-2 | 1.010 | 1.010306 | 1.009347 | 1.010 | 0.000499 |
| F-1-B-1 | 1.002516 | 1.002397 | 1.002516 | 1.002 | 6.92E-05 |
| F-2-B-1 | 1.009946 | 1.010425 | 1.010545 | 1.010 | 0.000317 |
| F-1-B-2 | 1.003475 | 1.002756 | 1.003595 | 1.003 | 0.000454 |
| F-2-B-2 | 8.435 | 8.437 | 8.438 | 8.437 | 0.001528 |

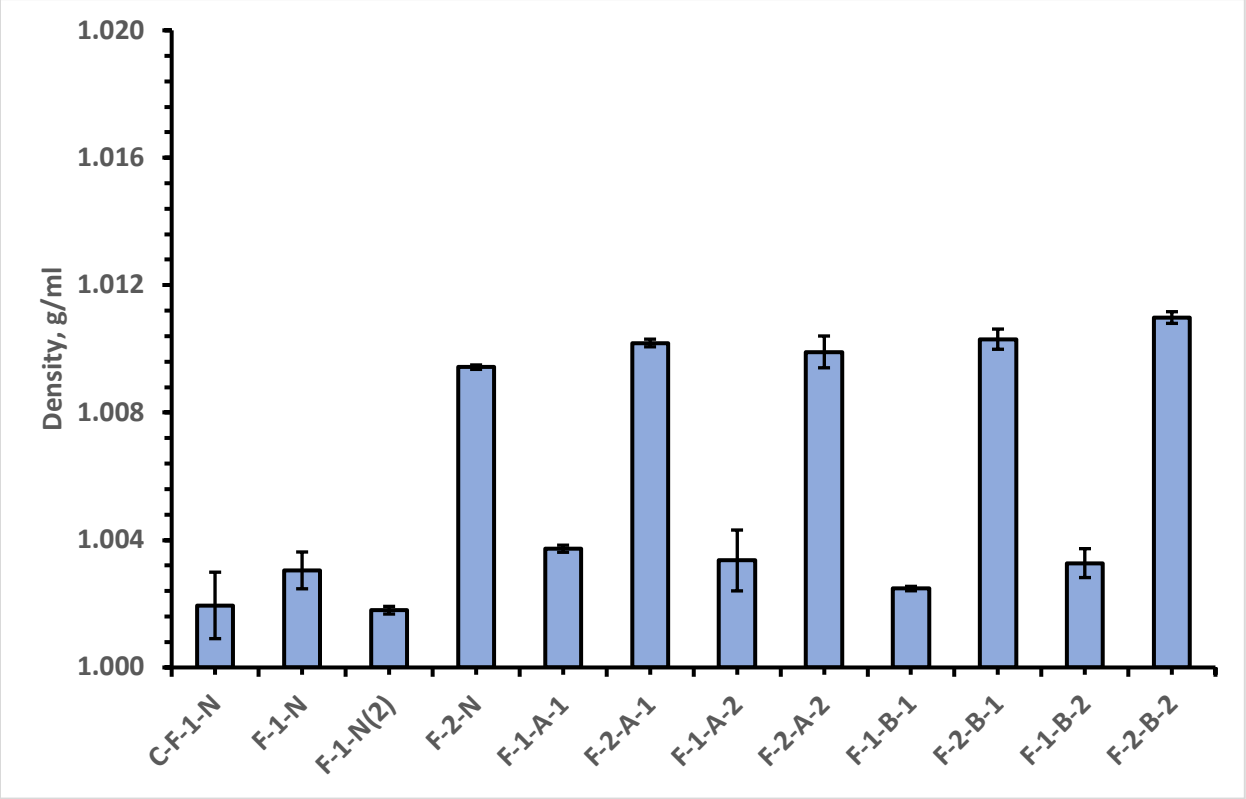


**Figure 4.1.2 – Density tested in accordance with ASTM D1475 (g/ml)**

Zeta potential

Table 4.1.3 summarizes the data for the zeta potential reported in mV of all samples. The test procedure used was outlines in Section 2.2.2.

**Table 4.1.3 – Zeta potential (mV)**

| Formula | Sample A | Sample B | Sample C | Average | Standard Deviation |
|---|---|---|---|---|---|
| C-F-1-A | 36.85 | 29.96 | 38.44 | 35.08 | 4.507597 |
| F-1-A | 38.34 | 32.07 | 38.34 | 36.25 | 3.619986 |
| F-1-A(2) | 33.42 | 26.26 | 36.31 | 32.00 | 5.173977 |
| F-2-A | 35.1 | 38.06 | 43.12 | 38.76 | 4.055564 |
| F-1-A-1 | -43.19 | -36.96 | -31.02 | -37.06 | 6.085576 |
| F-2-A-1 | -29.34 | -24.26 | -29.25 | -27.62 | 2.907307 |
| F-1-A-2 | -37.1 | -38.35 | -38.43 | -37.96 | 0.745855 |
| F-2-A-2 | -34.09 | -38.43 | -40.45 | -37.66 | 3.249759 |
| F-1-B-1 | -44.38 | -47.56 | -32.44 | -41.46 | 7.971725 |
| F-2-B-1 | -33.97 | -42.45 | -38.72 | -38.38 | 4.250212 |
| F-1-B-2 | -48.92 | -44.69 | -48.58 | -47.40 | 2.350199 |
| F-2-B-2 | -39.65 | -44.44 | -48.62 | -44.24 | 4.488456 |

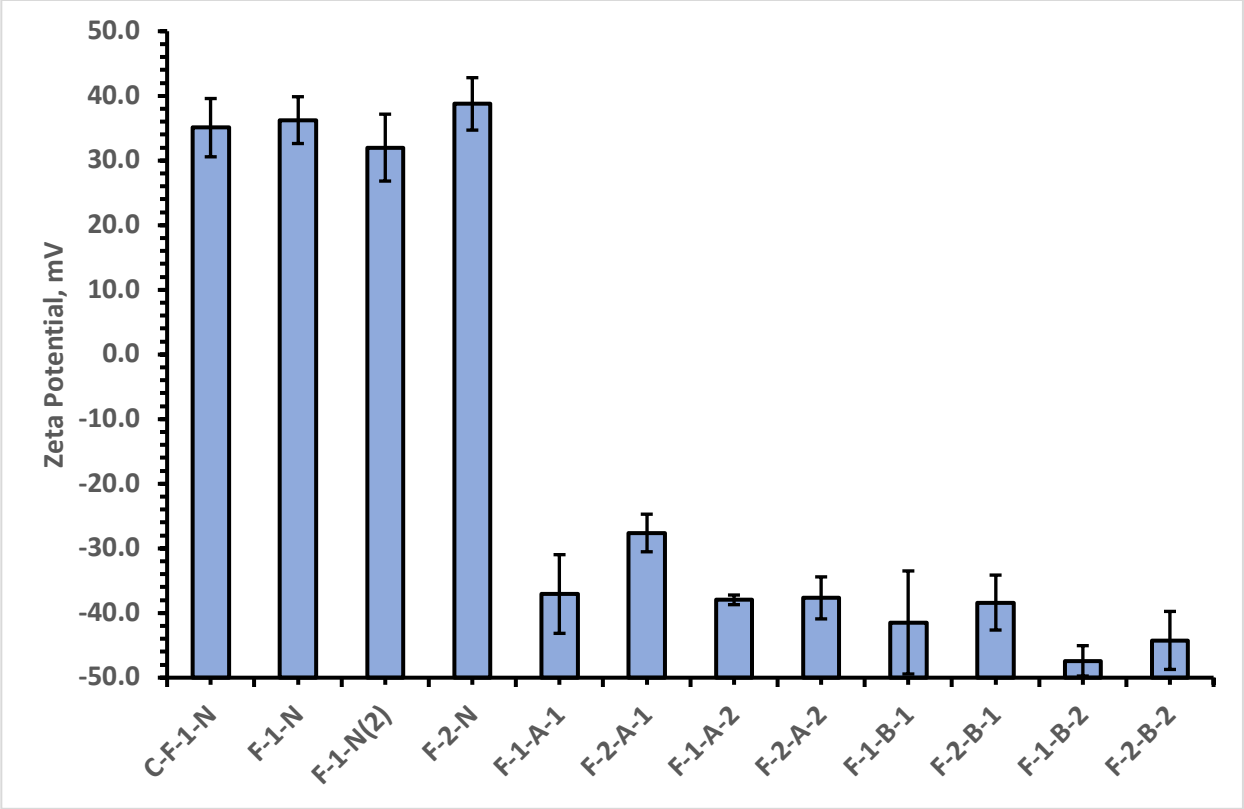


**Figure 4.1.3 – Zeta potential**

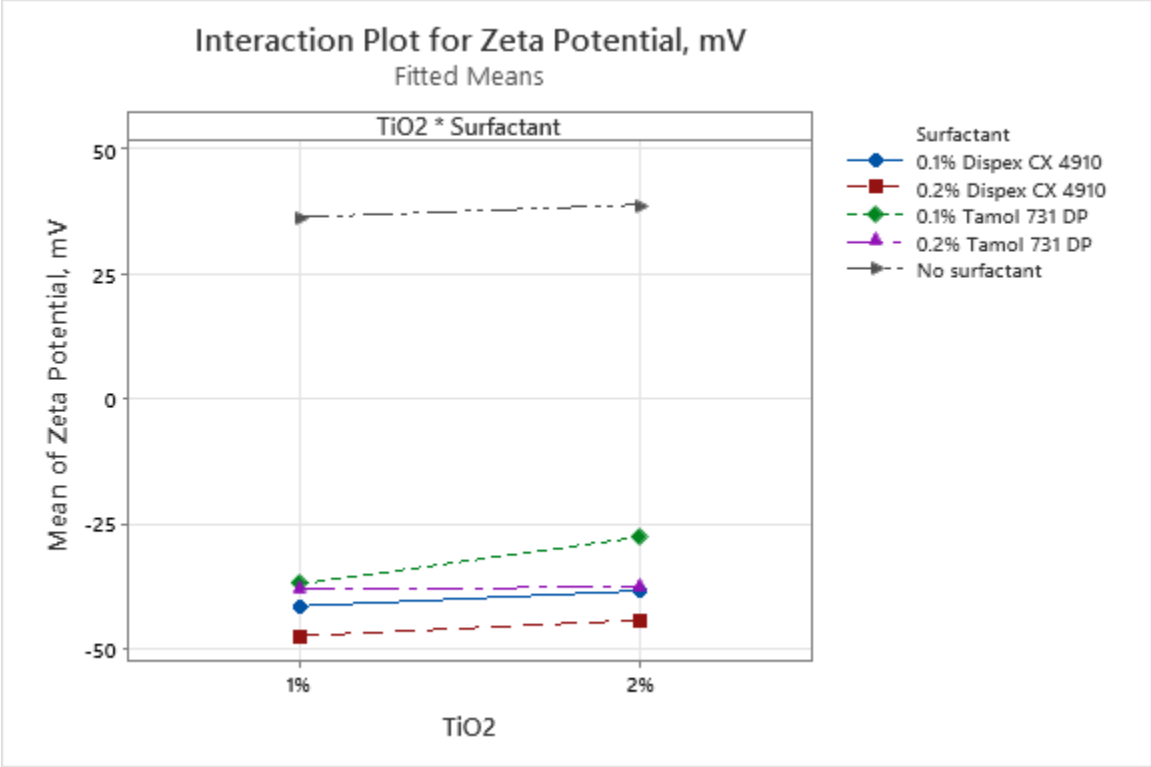


**Figure 4.14 – Interaction plot for zeta potential**

Particle size analysis and polydispersity

Tables 4.1.4 and 4.1.5 and Figures 4.1.5 and 4.1.6 summarize the effect of age on the particle size and polydispersity for C-F-1-N compositions produced without surfactant and without ultrasonication.

**Table 4.1.4 – Effect of age on particle size for C-F-1-N (nm)**

| Day | Sample A | Sample B | Sample C | Average | Standard Deviation |
|---|---|---|---|---|---|
| 0 | 328.8 | 395.5 | 317.4 | 347.2 | 42.187 |
| 8 | 317.9 | 367.7 | 326.8 | 337.5 | 26.558 |
| 27 | 331.6 | 415.8 | 300.3 | 349.2 | 59.735 |
| 42 | 330.7 | 539.8 | 296.6 | 389.0 | 131.676 |

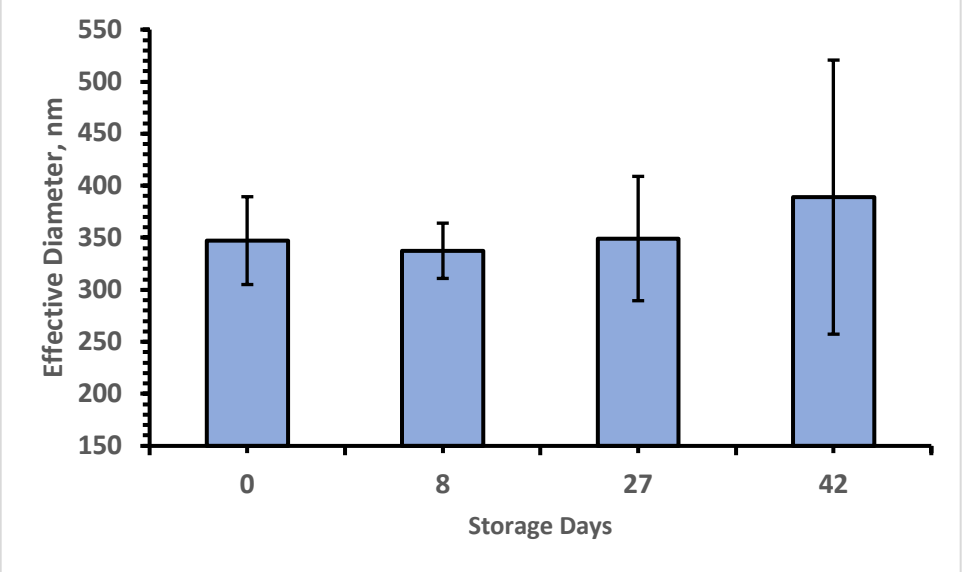


**Figure 4.1.5 – Effect of age on particle size for C-F-1-N**

**Table 4.1.5 – Effect of age on polydispersity for C-F-1-N**

| Day | Sample A | Sample B | Sample C | Average | Standard Deviation |
|---|---|---|---|---|---|
| 0 | 0.236 | 0.264 | 0.19 | 0.230 | 0.0374 |
| 8 | 0.203 | 0.328 | 0.238 | 0.256 | 0.0645 |
| 27 | 0.212 | 0.306 | 0.204 | 0.241 | 0.0567 |
| 42 | 0.225 | 0.347 | 0.253 | 0.275 | 0.0639 |

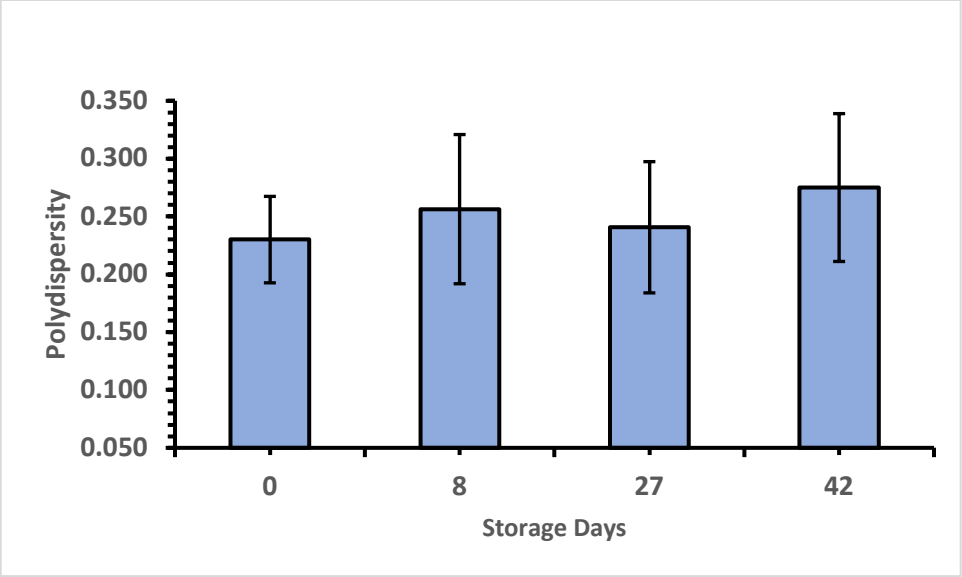


**Figure 4.1.6 – Effect of age on polydispersity for C-F-1-N**

Tables 4.1.6 and 4.1.7 and Figures 4.1.7 and 4.1.8 summarize the effect of age on the particle size and polydispersity for F-1-N (Same as C-F-1-N but ultrasonication as per Table 3.2.2 was used for preparation).

**Table 4.1.6 – Effect of age on particle size for F-1-N (nm)**

| Day | Sample A | Sample B | Sample C | Average | Standard Deviation |
|---|---|---|---|---|---|
| 5 | 177.9 | 185.7 | 187.2 | 183.6 | 4.993 |
| 11 | 187.8 | 171.5 | 177.4 | 178.9 | 8.253 |
| 21 | 180.8 | 174.4 | 183.4 | 179.5 | 4.632 |
| 28 | 173.9 | 172.2 | 175.2 | 173.8 | 1.504 |
| 47 | 181.8 | 174.6 | 180.1 | 178.8 | 3.763 |
| 62 | 183.2 | 180.7 | 183.3 | 182.4 | 1.473 |

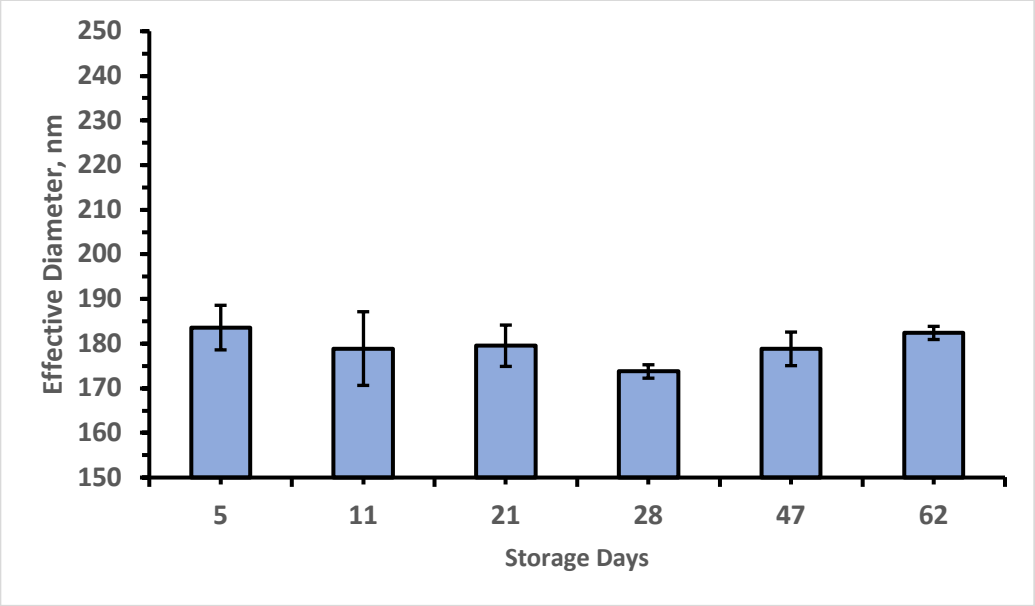


**Figure 4.1.7– Effect of age on particle size for F-1-N**

**Table 4.1.7 – Effect of age on polydispersity for F-1-N**

| Day | Sample A | Sample B | Sample C | Average | Standard Deviation |
|---|---|---|---|---|---|
| 5 | 0.080 | 0.172 | 0.190 | 0.147 | 0.0590 |
| 11 | 0.067 | 0.178 | 0.139 | 0.128 | 0.0563 |
| 21 | 0.180 | 0.171 | 0.165 | 0.172 | 0.0075 |
| 28 | 0.181 | 0.124 | 0.159 | 0.155 | 0.0287 |
| 47 | 0.174 | 0.149 | 0.164 | 0.162 | 0.0126 |
| 62 | 0.162 | 0.138 | 0.177 | 0.159 | 0.0197 |

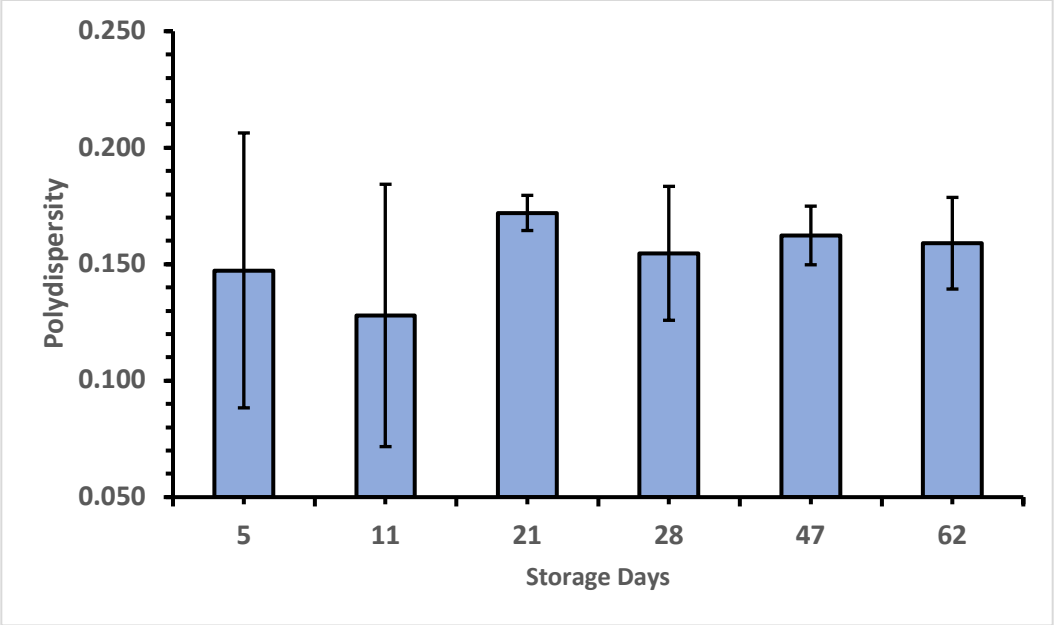


**Figure 4.1.8 – Effect of age on polydispersity for F-1-N**

Table 4.1.8 and Figure 4.1.9, as well as Table 4.1.9 and Figure 4.1.10 summarize the effect of age on the particle size and polydispersity, respectively, for F-1-N(2) (Same as F-1-N but mixing per Table 3.2.3 was used for preparation).

**Table 4.1.8 – Effect of age on particle size for F-1-N(2) (nm)**

| Day | Sample A | Sample B | Sample C | Average | Standard Deviation |
|---|---|---|---|---|---|
| 0 | 179.3 | 183.4 | 181.1 | 181.3 | 2.055 |
| 20 | 187.3 | 172.8 | 176.6 | 178.9 | 7.519 |
| 33 | 179.1 | 174.4 | 181.4 | 178.3 | 3.568 |

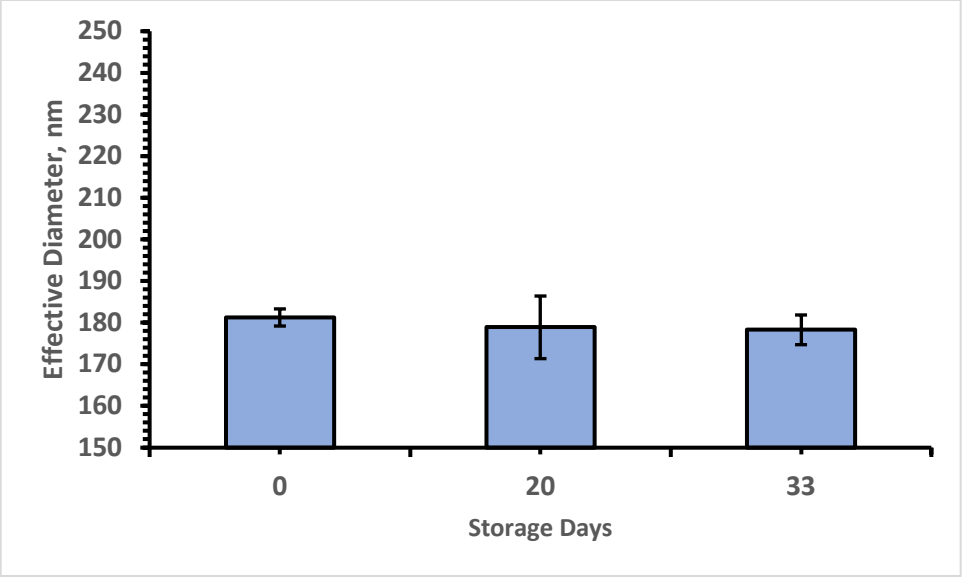


**Figure 4.1.9 – Effect of age on particle size for F-1-N(2)**

**Table 4.1.9 – Effect of age on polydispersity for F-1-N(2)**

| Day | Sample A | Sample B | Sample C | Average | Standard Deviation |
|---|---|---|---|---|---|
| 0 | 0.133 | 0.085 | 0.147 | 0.122 | 0.0325 |
| 20 | 0.151 | 0.122 | 0.139 | 0.137 | 0.0146 |
| 33 | 0.155 | 0.155 | 0.183 | 0.164 | 0.0162 |

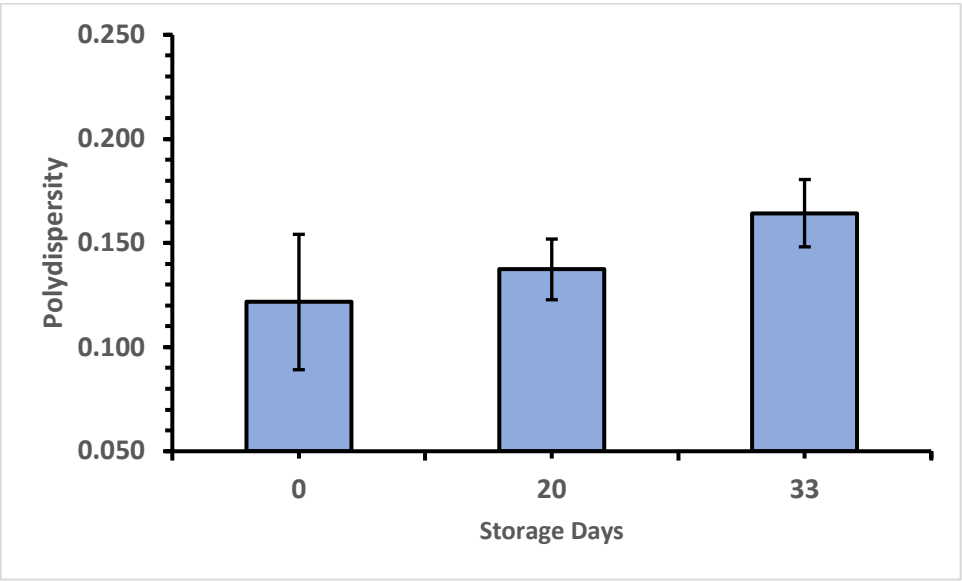


**Figure 4.1.10 – Effect of age on polydispersity for F-1-N(2)**

Table 4.1.10 and Figure 4.1.11, as well as Table 4.1.11 and Figure 4.1.12 summarize the effect of age on the particle size and polydispersity, respectively, for F-2-N.

**Table 4.1.10 – Effect of age on particle size for F-2-N (nm)**

| Day | Sample A | Sample B | Sample C | Average | Standard Deviation |
|---|---|---|---|---|---|
| 5 | 173.3 | 186.3 | 181.3 | 180.3 | 6.557 |
| 11 | 171.7 | 173.7 | 170.7 | 172.0 | 1.528 |
| 21 | 177.6 | 180.9 | 169.7 | 176.1 | 5.755 |
| 28 | 157.4 | 161.5 | 168.6 | 162.5 | 5.667 |
| 47 | 163.8 | 169.4 | 163.9 | 165.7 | 3.205 |
| 62 | 171.3 | 174.1 | 174.6 | 173.3 | 1.779 |

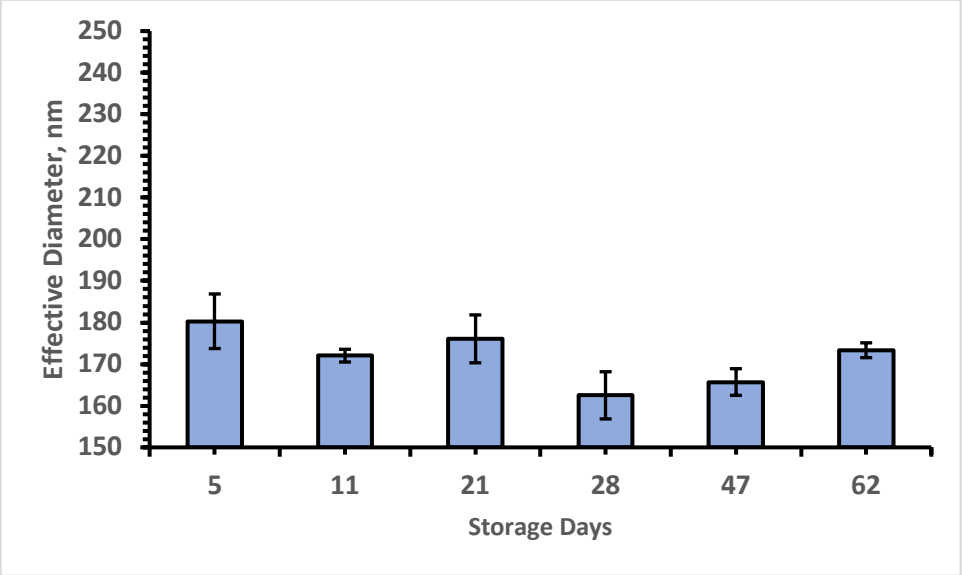


**Figure 4.1.11 – Effect of age on particle Size for F-2-N**

**Table 4.1.11 – Effect of age on polydispersity for F-2-N**

| Day | Sample A | Sample B | Sample C | Average | Stdev |
|---|---|---|---|---|---|
| 5 | 0.203 | 0.143 | 0.137 | 0.161 | 0.0365 |
| 11 | 0.174 | 0.152 | 0.197 | 0.174 | 0.0225 |
| 21 | 0.178 | 0.143 | 0.153 | 0.158 | 0.0180 |
| 28 | 0.241 | 0.18 | 0.214 | 0.212 | 0.0306 |
| 47 | 0.126 | 0.14 | 0.21 | 0.159 | 0.0450 |
| 62 | 0.194 | 0.18 | 0.167 | 0.180 | 0.0135 |

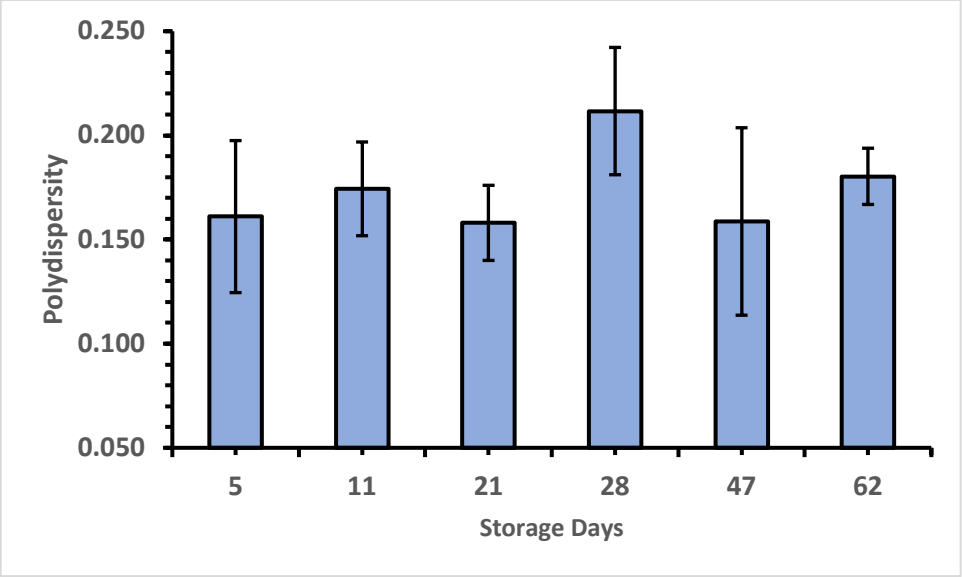


**Figure 4.1.12 – Effect of age on polydispersity for F-2-N**

Table 4.1.12 and Figures 4.1.13, as well as Table 4.1.13 and Figure 4.1.14 summarize the effect of age on the particle size and polydispersity, respectively, for F-1-A-1.

**Table 4.1.12 – Effect of age on particle size for F-1-A-1 (nm)**

| Day | Sample A | Sample B | Sample C | Average | Standard Deviation |
|---|---|---|---|---|---|
| 5 | 183.8 | 189.4 | 188 | 187.1 | 2.914 |
| 11 | 182.2 | 176.3 | 182.8 | 180.4 | 3.592 |
| 21 | 181.9 | 180.4 | 182.2 | 181.5 | 0.964 |
| 28 | 174.8 | 176.6 | 174.1 | 175.2 | 1.290 |
| 47 | 177.2 | 184.4 | 175.6 | 179.1 | 4.688 |
| 62 | 177.4 | 175.4 | 179.9 | 177.6 | 2.255 |

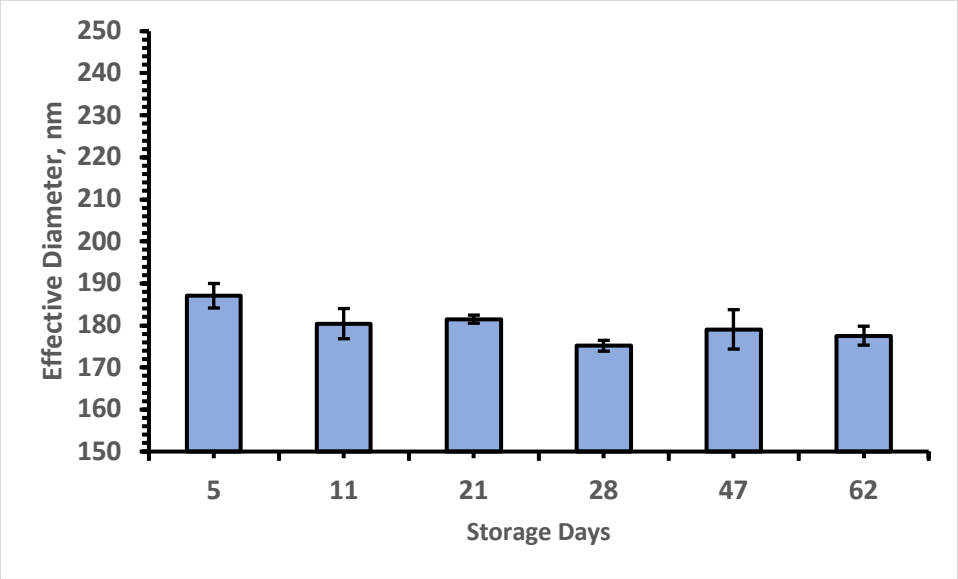


**Figure 4.1.13 – Effect of age on particle size for F-1-A-1**

**Table 4.1.13 – Effect of age on polydispersity for F-1-A-1**

| Day | Sample A | Sample B | Sample C | Average | Standard Deviation |
|---|---|---|---|---|---|
| 5 | 0.106 | 0.116 | 0.192 | 0.138 | 0.0470 |
| 11 | 0.177 | 0.15 | 0.165 | 0.164 | 0.0135 |
| 21 | 0.164 | 0.139 | 0.154 | 0.152 | 0.0126 |
| 28 | 0.126 | 0.167 | 0.088 | 0.127 | 0.0395 |
| 47 | 0.141 | 0.068 | 0.171 | 0.127 | 0.0530 |
| 62 | 0.146 | 0.089 | 0.139 | 0.125 | 0.0311 |

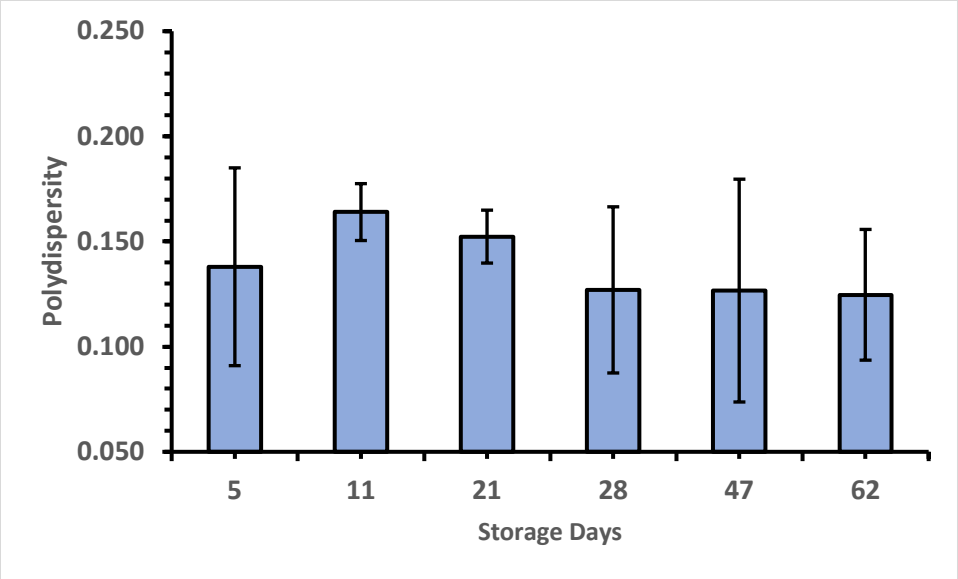


**Figure 4.1.14 – Effect of age on polydispersity for F-1-A-1**

Table 4.1.14 and Figure 4.1.15, as well as Table 4.1.15 and Figure 4.1.16 summarize the effect of age on the particle size and polydispersity, respectively, for F-2-A-1.

**Table 4.1.14 – Effect of age on particle size for F-2-A-1 (nm)**

| Day | Sample A | Sample B | Sample C | Average | Standard Deviation |
|---|---|---|---|---|---|
| 5 | 179 | 186.7 | 184.9 | 183.5 | 4.028 |
| 11 | 169.9 | 167.1 | 173.5 | 170.2 | 3.208 |
| 21 | 181 | 167.4 | 179 | 175.8 | 7.343 |
| 28 | 165 | 163 | 169.2 | 165.7 | 3.164 |
| 47 | 178.9 | 170.3 | 172.7 | 174.0 | 4.438 |
| 62 | 174.9 | 173.7 | 169.8 | 172.8 | 2.666 |

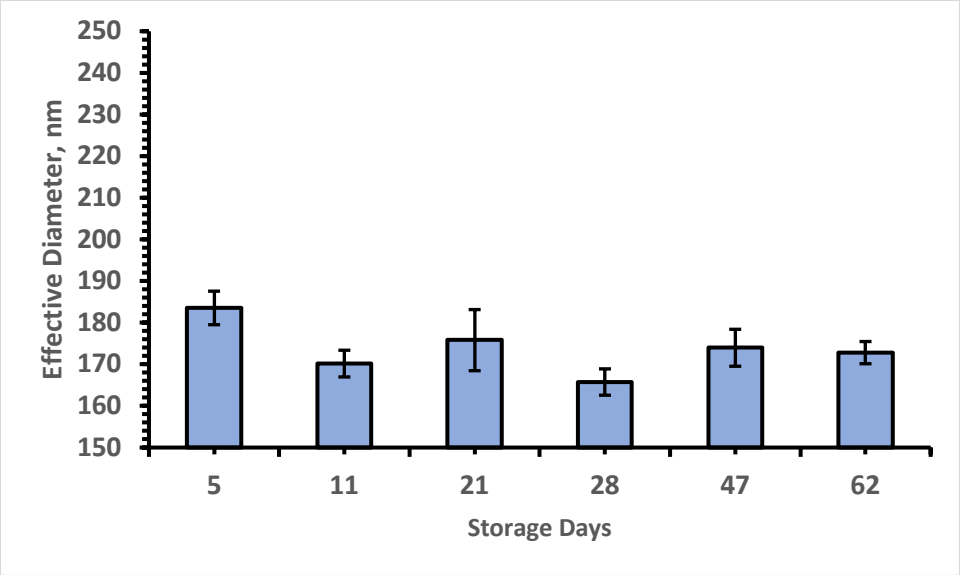


**Figure 4.1.15 – Effect of age on particle size for F-2-A-1**

**Table 4.1.15 – Effect of age on polydispersity for F-2-A-1**

| Day | Sample A | Sample B | Sample C | Average | Standard Deviation |
|---|---|---|---|---|---|
| 5 | 0.14 | 0.128 | 0.21 | 0.159 | 0.0443 |
| 11 | 0.16 | 0.214 | 0.171 | 0.182 | 0.0285 |
| 21 | 0.163 | 0.17 | 0.191 | 0.175 | 0.0146 |
| 28 | 0.195 | 0.19 | 0.193 | 0.193 | 0.0025 |
| 47 | 0.142 | 0.184 | 0.145 | 0.157 | 0.0234 |
| 62 | 0.201 | 0.16 | 0.189 | 0.183 | 0.0211 |

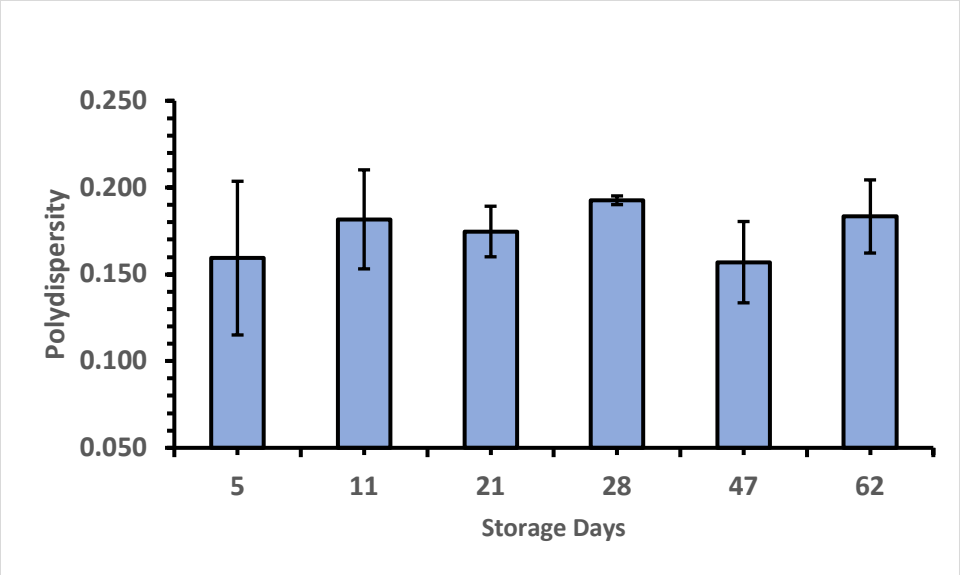


**Figure 4.1.16 – Effect of age on polydispersity for F-2-A-1**

Table 4.1.16 and Figure 4.1.17, as well as Table 4.1.17 and Figure 4.1.18 summarize the effect of age on the particle size and polydispersity, respectively, for F-1-A-2.

**Table 4.1.16 – Effect of age on particle size for F-1-A-2 (nm)**

| Day | Sample A | Sample B | Sample C | Average | Standard Deviation |
|---|---|---|---|---|---|
| 0 | 194.8 | 187.7 | 191.7 | 191.4 | 3.559 |
| 8 | 194.9 | 190.8 | 185.5 | 190.4 | 4.713 |
| 27 | 201.2 | 186.7 | 200.8 | 196.2 | 8.259 |
| 42 | 195.6 | 188.3 | 190.4 | 191.4 | 3.758 |

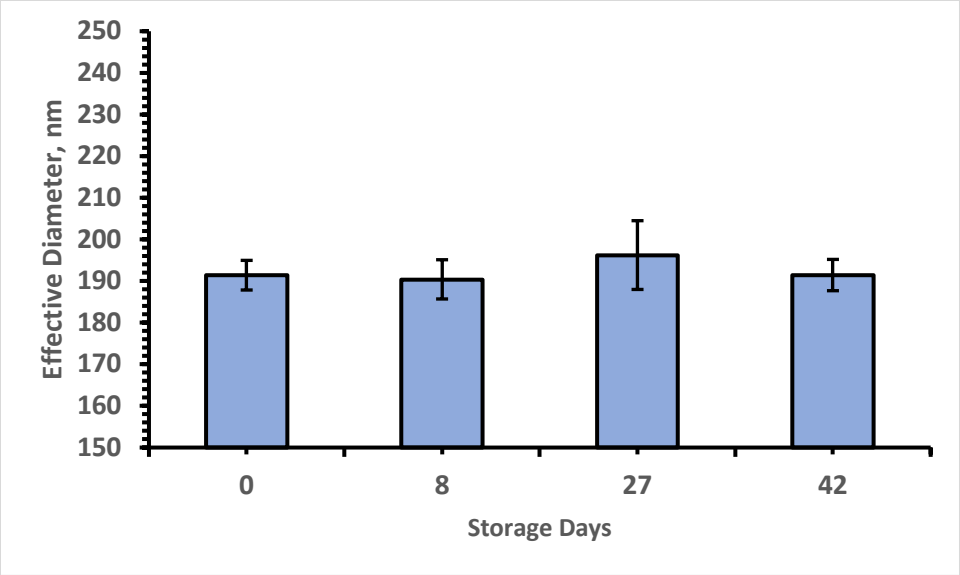


**Figure 4.1.17 – Effect of age on particle size for F-1-A-2**

**Table 4.1.17 – Effect of age on polydispersity for F-1-A-2**

| Day | Sample A | Sample B | Sample C | Average | Standard Deviation |
|---|---|---|---|---|---|
| 0 | 0.164 | 0.194 | 0.078 | 0.145 | 0.0602 |
| 8 | 0.182 | 0.158 | 0.101 | 0.147 | 0.0416 |
| 27 | 0.18 | 0.084 | 0.122 | 0.129 | 0.0483 |
| 42 | 0.197 | 0.155 | 0.182 | 0.178 | 0.0213 |

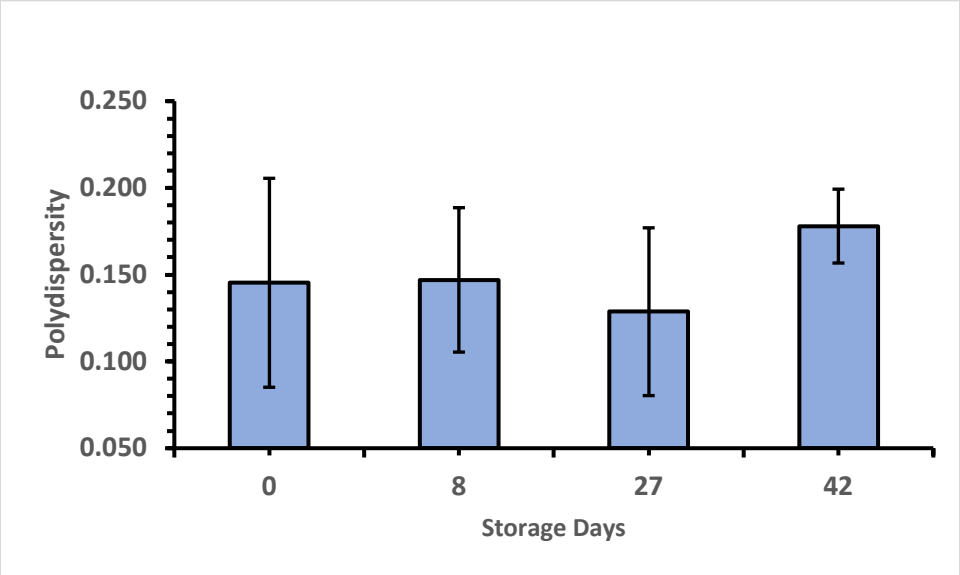


**Figure 4.1.18 – Effect of age on polydispersity for F-1-A-2**

Table 4.1.18 and Figure 4.1.19, as well as Table 4.1.19 and Figure 4.1.20 summarize the effect of age on the particle size and polydispersity, respectively, for F-2-A-2.

**Table 4.1.18 – Effect of age on particle size for F-2-A-2 (nm)**

| Day | Sample A | Sample B | Sample C | Average | Standard Deviation |
|---|---|---|---|---|---|
| 0 | 191.5 | 182.5 | 169.4 | 181.1 | 11.113 |
| 8 | 184.1 | 179.2 | N/A | 181.7 | 3.465 |
| 27 | 197.1 | 193 | N/A | 195.1 | 2.899 |
| 42 | 196 | 188.5 | N/A | 192.3 | 5.303 |

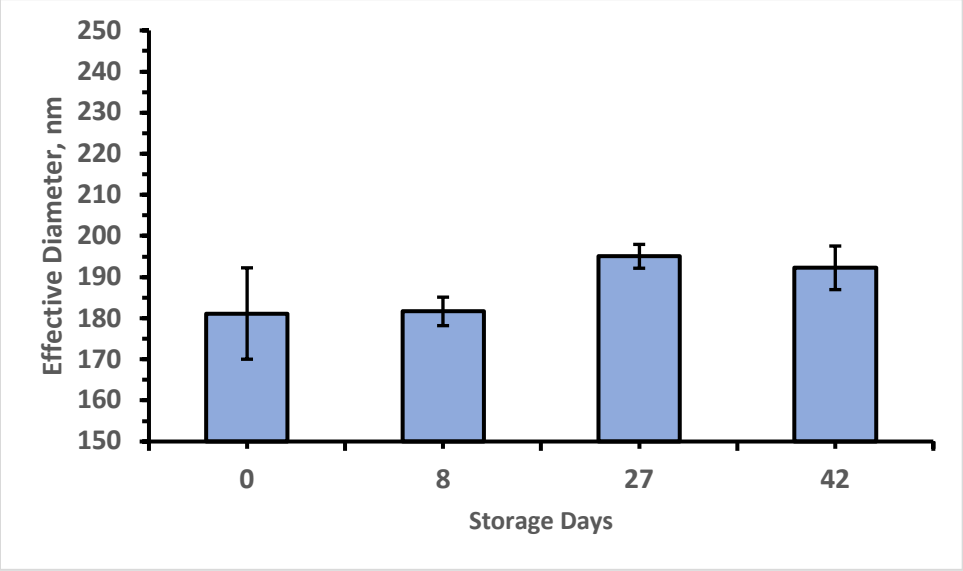


**Figure 4.1.19 – Effect of age on particle size for F-2-A-2**

**Table 4.1.19 – Effect of age on polydispersity for F-2-A-2**

| Day | Sample A | Sample B | Sample C | Average | Standard Deviation |
|---|---|---|---|---|---|
| 0 | 0.197 | 0.214 | 0.168 | 0.193 | 0.0233 |
| 8 | 0.214 | 0.193 | N/A | 0.204 | 0.0148 |
| 27 | 0.162 | 0.177 | N/A | 0.170 | 0.0106 |
| 42 | 0.199 | 0.135 | N/A | 0.167 | 0.0453 |

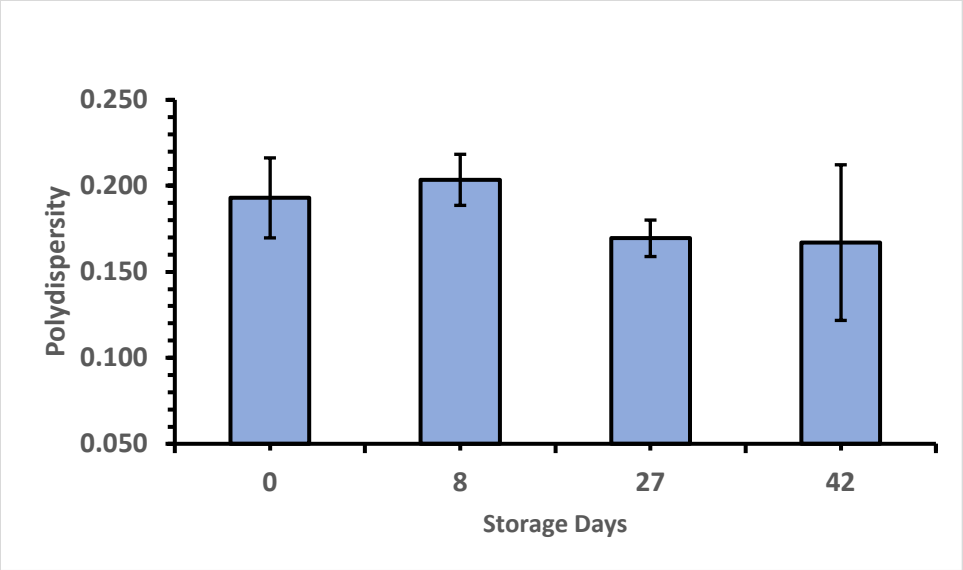


**Figure 4.1.20 – Effect of age on polydispersity for F-2-A-2**

Table 4.1.20 and Figure 4.1.21, as well as Table 4.1.21 and Figure 4.1.22 summarize the effect of age on the particle size and polydispersity, respectively, for F-1-B-1.

**Table 4.1.20 – Effect of age on particle size for F-1-B-1 (nm)**

| Day | Sample A | Sample B | Sample C | Average | Standard Deviation |
|---|---|---|---|---|---|
| 0 | 182.6 | 185.6 | 187.9 | 185.4 | 2.658 |
| 20 | 186.8 | 184.7 | 182.1 | 184.5 | 2.354 |
| 33 | 186.5 | 191.2 | 189.9 | 189.2 | 2.427 |

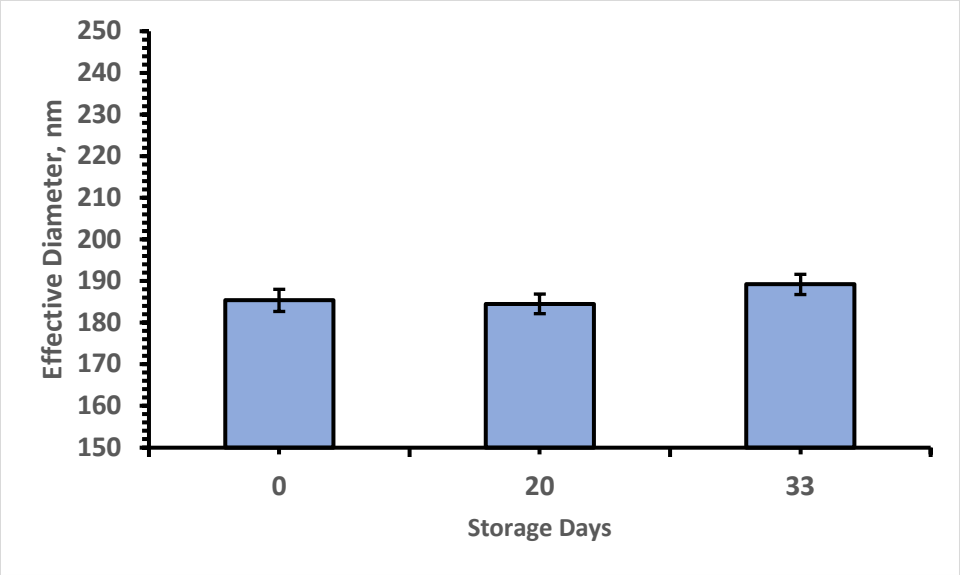


**Figure 4.1.21 – Effect of age on particle size for F-1-B-1**

**Table 4.1.21 – Effect of age on polydispersity for F-1-B-1**

| Day | Sample A | Sample B | Sample C | Average | Standard Deviation |
|---|---|---|---|---|---|
| 0 | 0.130 | 0.165 | 0.142 | 0.146 | 0.0178 |
| 20 | 0.161 | 0.088 | 0.149 | 0.133 | 0.0391 |
| 33 | 0.143 | 0.145 | 0.121 | 0.136 | 0.0133 |

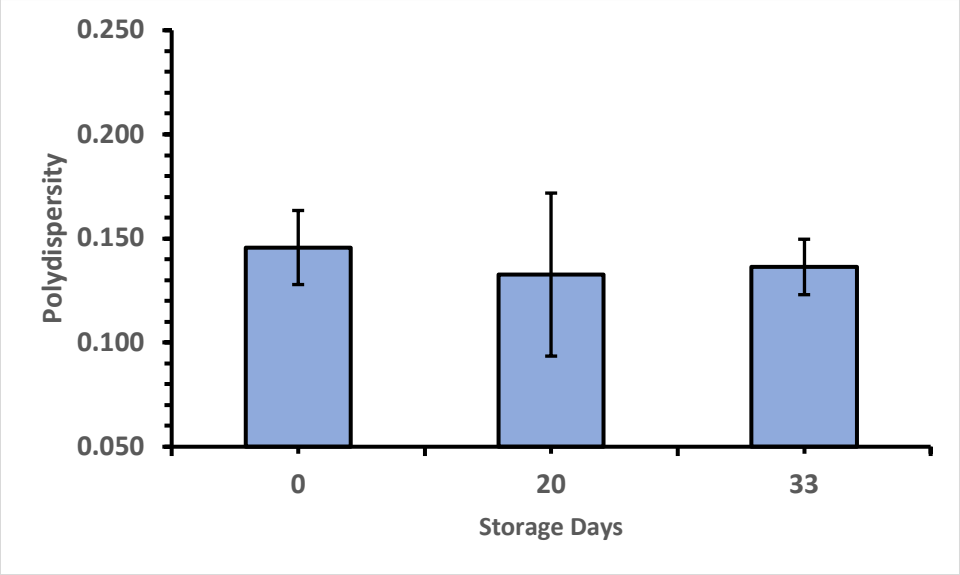


**Figure 4.1.22 – Effect of age on polydispersity for F-1-B-1**

Table 4.1.22 and Figure 4.1.23, as well as Table 4.1.23 and Figure 4.1.24 summarize the effect of age on the particle size and polydispersity, respectively, for F-2-B-1.

**Table 4.1.22 – Effect of age on particle size for F-2-B-1 (nm)**

| Day | Sample A | Sample B | Sample C | Average | Standard Deviation |
|---|---|---|---|---|---|
| 0 | 174.3 | 179.8 | 174.6 | 176.2 | 3.092 |
| 19 | 178.9 | 179 | 178.7 | 178.9 | 0.153 |
| 32 | 177.6 | 183.1 | 180.7 | 180.5 | 2.757 |

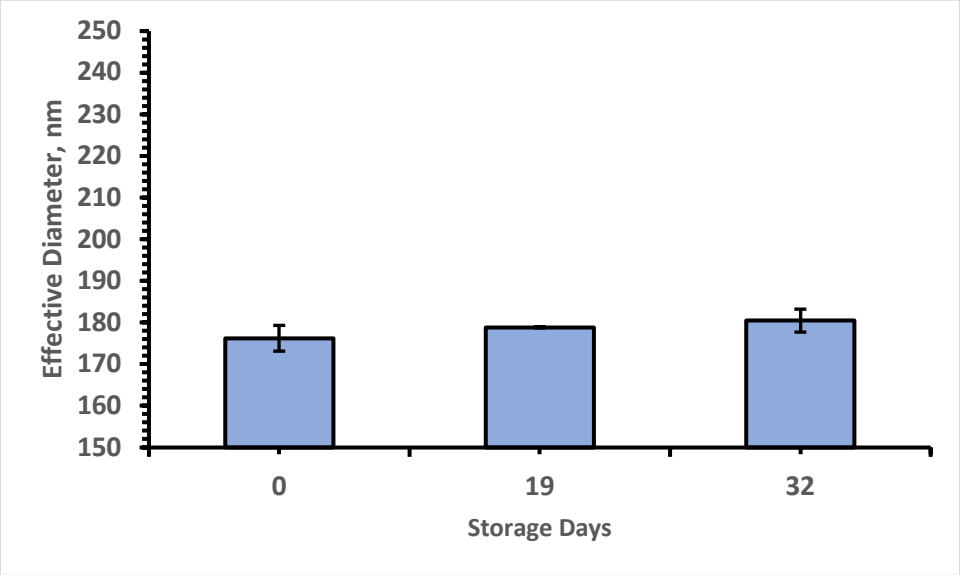


**Figure 4.1.23 – Effect of age on particle size for F-2-B-1**

**Table 4.1.23 – Effect of age on polydispersity for F-2-B-1**

| Day | Sample A | Sample B | Sample C | Average | Standard Deviation |
|---|---|---|---|---|---|
| 0 | 0.213 | 0.135 | 0.185 | 0.178 | 0.0395 |
| 19 | 0.141 | 0.154 | 0.216 | 0.170 | 0.0401 |
| 32 | 0.134 | 0.125 | 0.154 | 0.138 | 0.0148 |

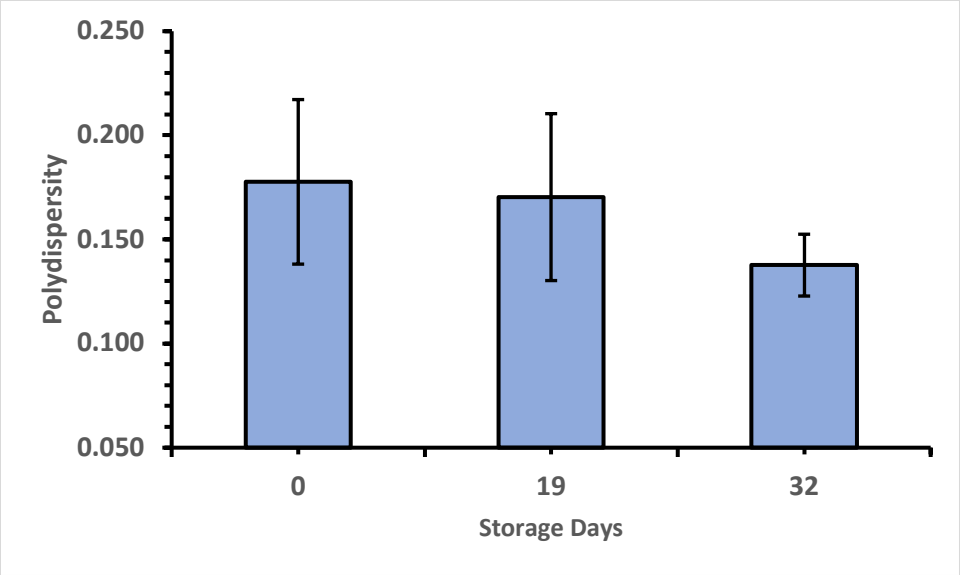


**Figure 4.1.24 – Effect of age on polydispersity for F-2-B-1**

Table 4.1.24 and Figure 4.1.25, as well as Table 4.1.25 and Figure 4.1.26 summarize the effect of age on the particle size and polydispersity, respectively, for F-1-B-2.

**Table 4.1.24 – Effect of age on particle size for F-1-B-2 (nm)**

| Day | Sample A | Sample B | Sample C | Average | Standard Deviation |
|---|---|---|---|---|---|
| 0 | 191.9 | 203 | 197.7 | 197.5 | 5.552 |
| 19 | 224.9 | 231.5 | 215.5 | 224.0 | 8.041 |
| 32 | 220.1 | 222.4 | 219 | 220.5 | 1.735 |

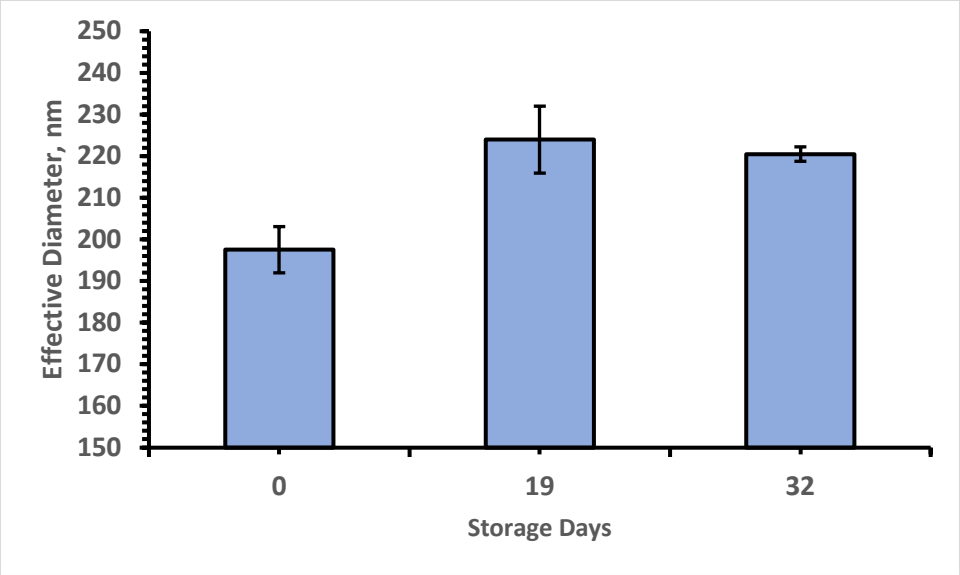


**Figure 4.1.25 – Effect of age on particle size for F-1-B-2**

**Table 4.1.25 – Effect of age on polydispersity for F-1-B-2**

| Day | Sample A | Sample B | Sample C | Average | Standard Deviation |
|---|---|---|---|---|---|
| 0 | 0.189 | 0.102 | 0.140 | 0.144 | 0.0436 |
| 19 | 0.181 | 0.186 | 0.204 | 0.190 | 0.0121 |
| 32 | 0.205 | 0.223 | 0.165 | 0.198 | 0.0297 |

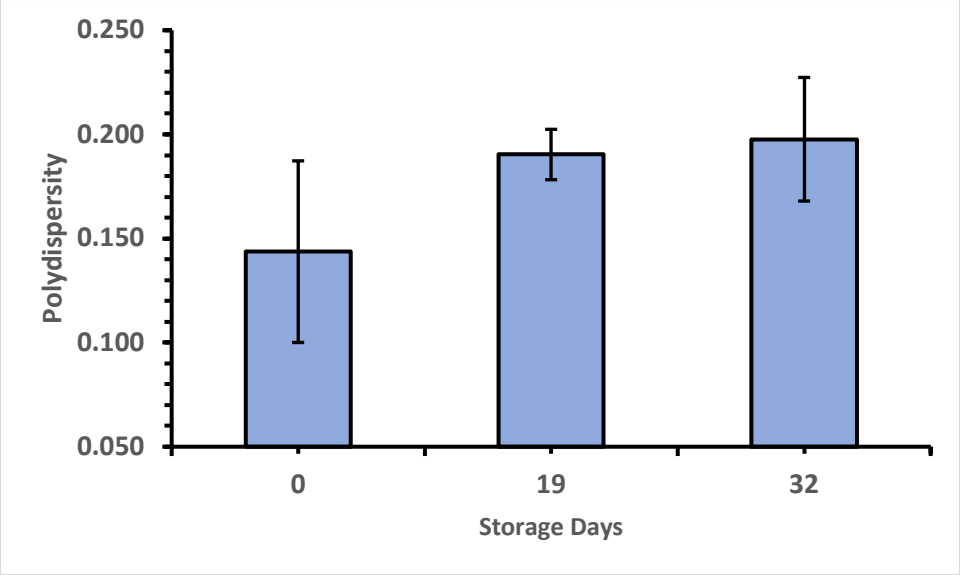


**Figure 4.1.26 – Effect of age on polydispersity for F-1-B-2**

Table 4.1.26 and Figure 4.1.27, as well as Table 4.1.27 and Figure 4.1.28 summarize the effect of age on the particle size and polydispersity, respectively, for F-2-B-2.

**Table 4.1.26 – Effect of age on particle size for F-2-B-2 (nm)**

| Day | Sample A | Sample B | Sample C | Average | Standard Deviation |
|---|---|---|---|---|---|
| 0 | 181.1 | 186 | 179.7 | 182.3 | 3.308 |
| 19 | 191.1 | 183 | 200.2 | 191.4 | 8.605 |
| 32 | 194.1 | 198.4 | 196.7 | 196.4 | 2.166 |

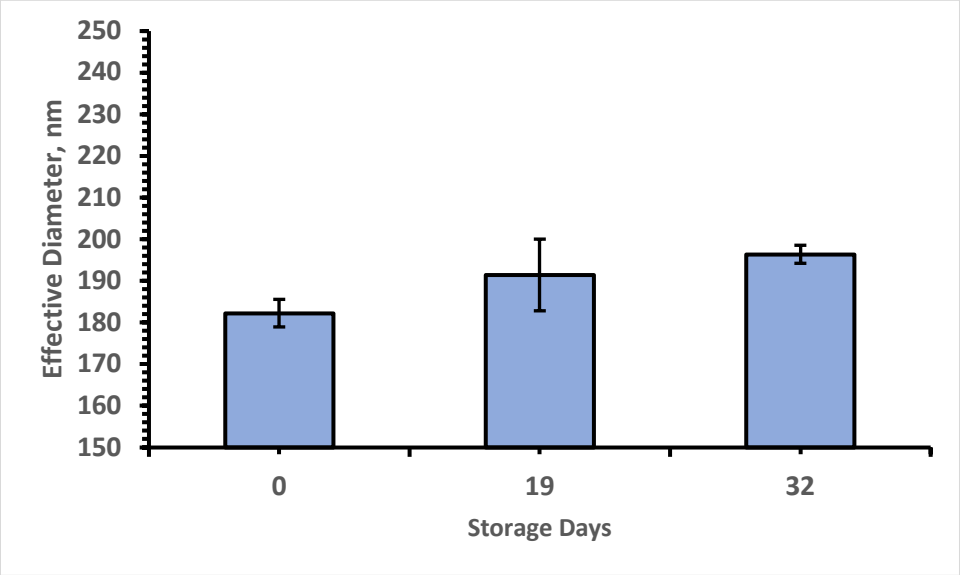


**Figure 4.1.27 – Effect of age on particle size for F-2-B-2**

**Table 4.1.27 – Effect of age on polydispersity for F-2-B-2**

| Day | Sample A | Sample B | Sample C | Average | Standard Deviation |
|---|---|---|---|---|---|
| 0 | 0.157 | 0.112 | 0.167 | 0.145 | 0.0293 |
| 19 | 0.167 | 0.194 | 0.187 | 0.183 | 0.0140 |
| 32 | 0.159 | 0.194 | 0.203 | 0.185 | 0.0232 |

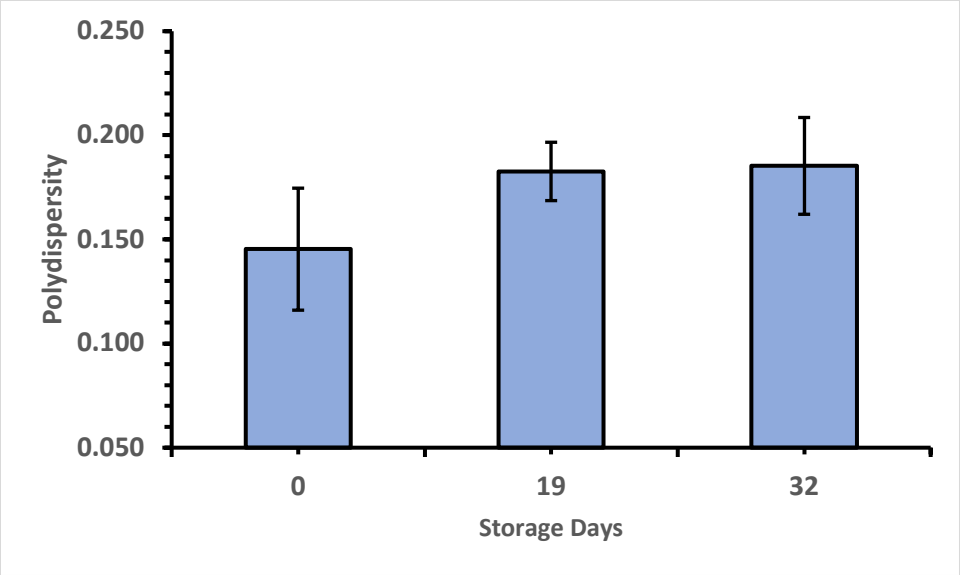


**Figure 4.1.28 – Effect of age on polydispersity for F-2-B-2**

Tables 4.1.28 and 4.1.29 summarize the particle size of investigated samples at 3±3 days and 30±3 days, respectively. Tables 4.1.30 and 4.1.31 summarize the polydispersity of the samples at 3±3 days and 30±3 days, respectively. Figures 4.1.29 and 4.1.32 summarize the particle size at 3±3 days vs 30±3 and polydispersity at 3±3 days vs 30±3, respectively. Figures 4.1.30, 4.1.31, 4.1.33 and 4.1.34 are the interaction plots for particle size at 3±3 days, particle size at 30±3 days, polydispersity at 3±3 days, polydispersity at 30±3 days and zeta potential, respectively.

**Table 4.1.28 – Effective diameter (in nm) at the age of at 3±3 days**

| Formula | Sample A | Sample B | Sample C | Average | Standard Deviation |
|---|---|---|---|---|---|
| C-F-1-N | 328.8 | 395.5 | 317.4 | 347.2 | 42.187 |
| F-1-N | 177.9 | 185.7 | 187.2 | 183.6 | 4.993 |
| F-1-N(2) | 179.3 | 183.4 | 181.1 | 181.3 | 2.055 |
| F-2-N | 173.3 | 186.3 | 181.3 | 180.3 | 6.557 |
| F-1-A-1 | 183.8 | 189.4 | 188.0 | 187.1 | 2.914 |
| F-2-A-1 | 179.0 | 186.7 | 184.9 | 183.5 | 4.028 |
| F-1-A-2 | 194.8 | 187.7 | 191.7 | 191.4 | 3.559 |
| F-2-A-2 | 191.5 | 182.5 | 169.4 | 181.1 | 11.113 |
| F-1-B-1 | 182.6 | 185.6 | 187.9 | 185.4 | 2.658 |
| F-2-B-1 | 174.3 | 179.8 | 174.6 | 176.2 | 3.092 |
| F-1-B-2 | 191.9 | 203.0 | 197.7 | 197.5 | 5.552 |
| F-2-B-2 | 181.1 | 186.0 | 179.7 | 182.3 | 3.308 |

**Table 4.1.29 – Effective diameter (in nm) at the age of 30±3 days**

| Formula | Sample A | Sample B | Sample C | Average | Standard Deviation |
|---|---|---|---|---|---|
| C-F-1-N | 331.6 | 415.8 | 300.3 | 349.2 | 59.735 |
| F-1-N | 173.9 | 172.2 | 175.2 | 173.8 | 1.504 |
| F-1-N(2) | 179.1 | 174.4 | 181.4 | 178.3 | 3.568 |
| F-2-N | 157.4 | 161.5 | 168.6 | 162.5 | 5.667 |
| F-1-A-1 | 174.8 | 176.6 | 174.1 | 175.2 | 1.290 |
| F-2-A-1 | 165.0 | 163.0 | 169.2 | 165.7 | 3.164 |
| F-1-A-2 | 201.2 | 186.7 | 200.8 | 196.2 | 8.259 |
| F-2-A-2 | 197.1 | 193.0 | 168.9 | 186.3 | 15.236 |
| F-1-B-1 | 186.5 | 191.2 | 189.9 | 189.2 | 2.427 |
| F-2-B-1 | 177.6 | 183.1 | 180.7 | 180.5 | 2.757 |
| F-1-B-2 | 220.1 | 222.4 | 219.0 | 220.5 | 1.735 |
| F-2-B-2 | 194.1 | 198.4 | 196.7 | 196.4 | 2.166 |

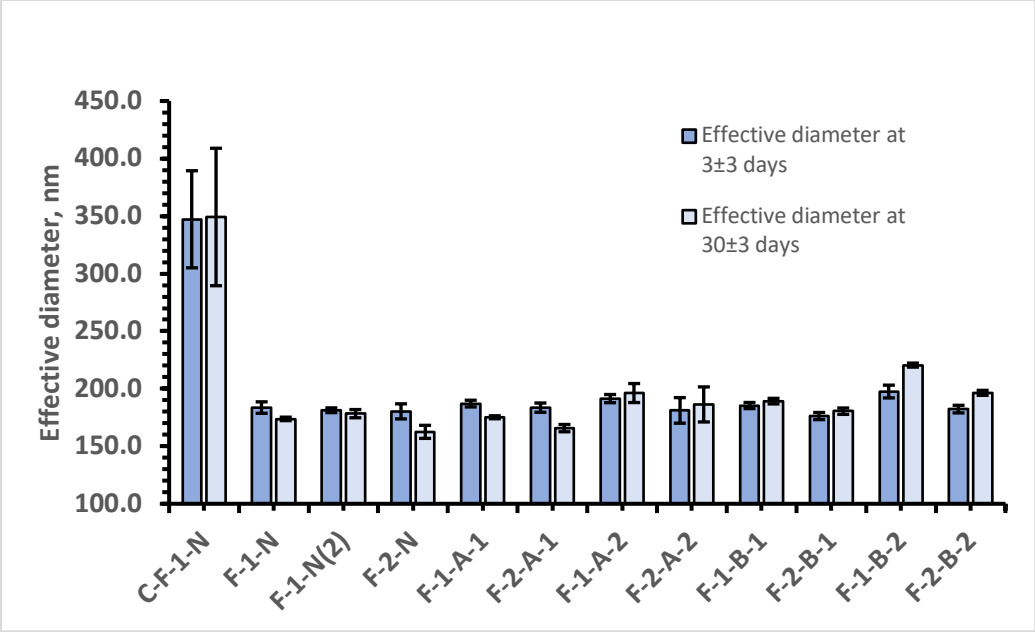


**Figure 4.1.29 – Particle size at 3±3 vs. 30±3 days**

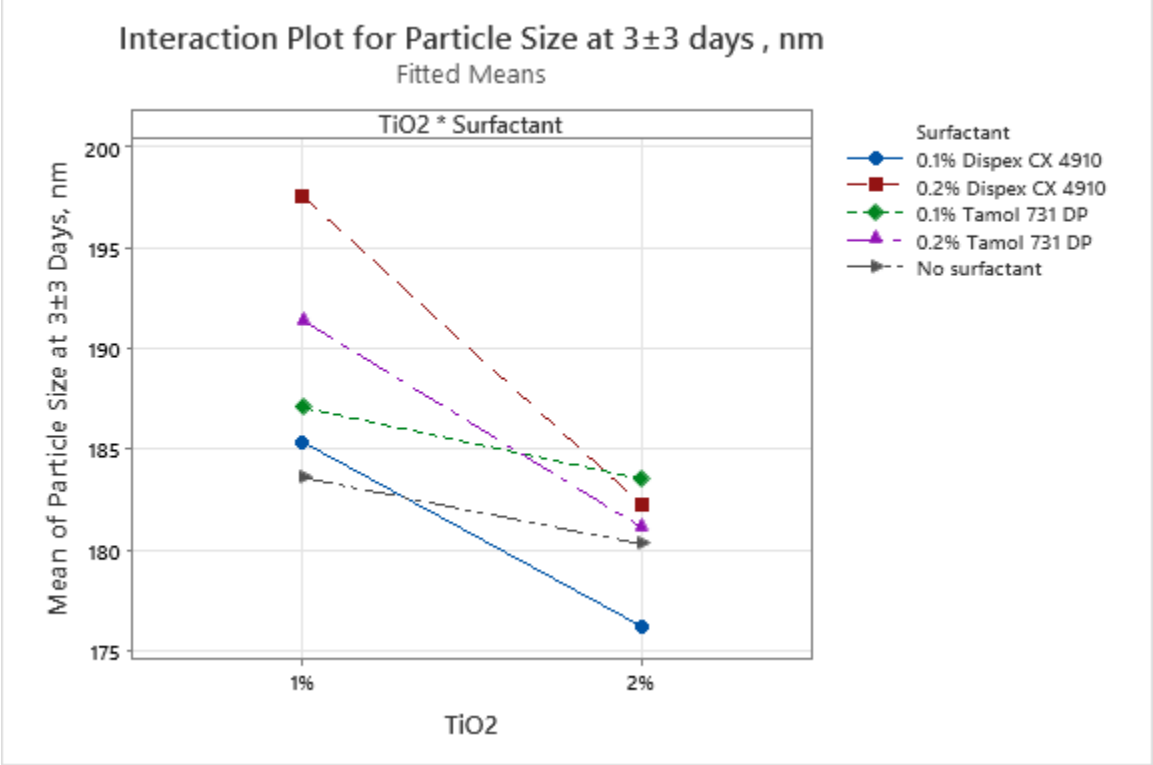


**Figure 4.1.30 – Interaction Plot for Particle Size at 3±3 Days**

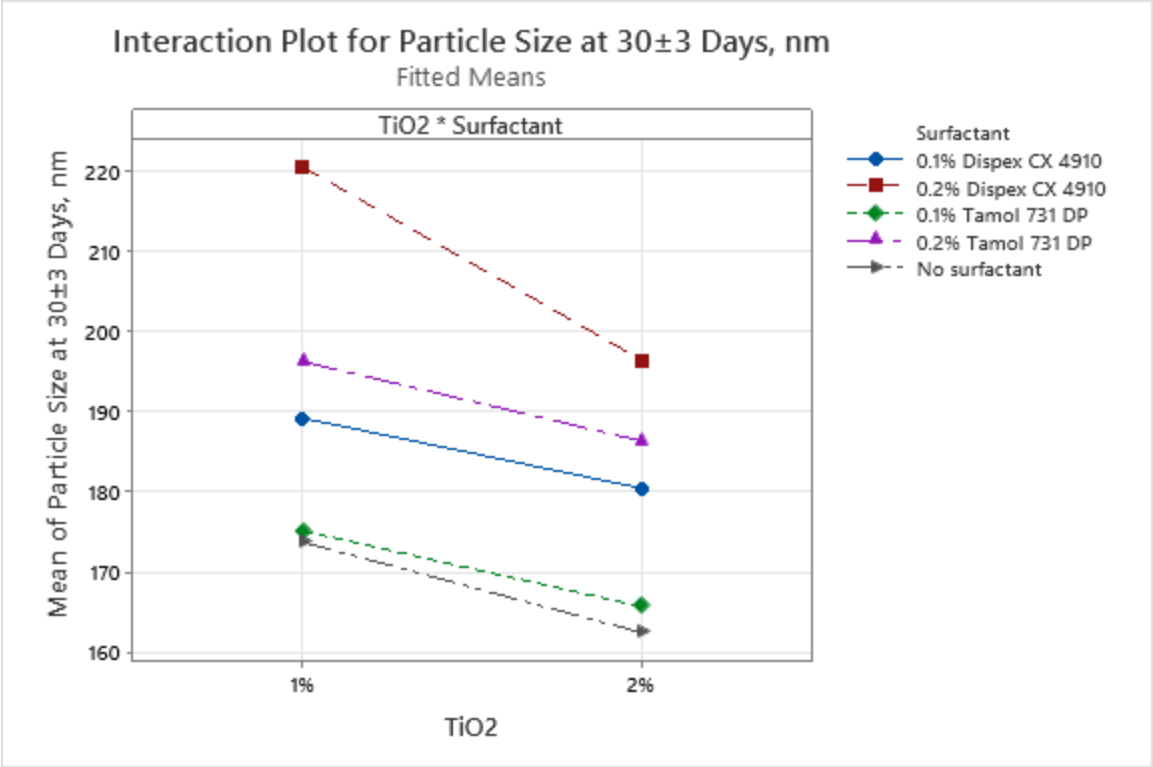


**Figure 4.1.31 – Interaction Plot for Particle Size at 30±3 Days**

**Table 4.1.30 – Polydispersity at the age of 3±3 days**

| Formula | Sample A | Sample B | Sample C | Average | Standard Deviation |
|---|---|---|---|---|---|
| C-F-1-N | 0.236 | 0.264 | 0.190 | 0.230 | 0.037 |
| F-1-N | 0.080 | 0.172 | 0.190 | 0.147 | 0.059 |
| F-1-N(2) | 0.133 | 0.085 | 0.147 | 0.122 | 0.033 |
| F-2-N | 0.203 | 0.143 | 0.137 | 0.161 | 0.036 |
| F-1-A-1 | 0.106 | 0.116 | 0.192 | 0.138 | 0.047 |
| F-2-A-1 | 0.140 | 0.128 | 0.210 | 0.159 | 0.044 |
| F-1-A-2 | 0.164 | 0.194 | 0.078 | 0.145 | 0.060 |
| F-2-A-2 | 0.197 | 0.214 | 0.168 | 0.193 | 0.023 |
| F-1-B-1 | 0.130 | 0.165 | 0.142 | 0.146 | 0.018 |
| F-2-B-1 | 0.213 | 0.135 | 0.185 | 0.178 | 0.040 |
| F-1-B-2 | 0.189 | 0.102 | 0.140 | 0.144 | 0.044 |
| F-2-B-2 | 0.157 | 0.112 | 0.167 | 0.145 | 0.029 |

**Table 4.1.31– Polydispersity at the age of 30±3 days**

| Formula | Sample A | Sample B | Sample C | Average | Standard Deviation |
|---|---|---|---|---|---|
| C-F-1-N | 0.212 | 0.306 | 0.204 | 0.241 | 0.057 |
| F-1-N | 0.181 | 0.124 | 0.159 | 0.155 | 0.029 |
| F-1-N(2) | 0.155 | 0.155 | 0.183 | 0.164 | 0.016 |
| F-2-N | 0.241 | 0.180 | 0.214 | 0.212 | 0.031 |
| F-1-A-1 | 0.126 | 0.167 | 0.088 | 0.127 | 0.040 |
| F-2-A-1 | 0.195 | 0.190 | 0.193 | 0.193 | 0.003 |
| F-1-A-2 | 0.180 | 0.084 | 0.122 | 0.129 | 0.048 |
| F-2-A-2 | 0.162 | 0.177 | 0.199 | 0.179 | 0.019 |
| F-1-B-1 | 0.143 | 0.145 | 0.121 | 0.136 | 0.013 |
| F-2-B-1 | 0.134 | 0.125 | 0.154 | 0.138 | 0.015 |
| F-1-B-2 | 0.205 | 0.223 | 0.165 | 0.198 | 0.030 |
| F-2-B-2 | 0.159 | 0.194 | 0.203 | 0.185 | 0.023 |

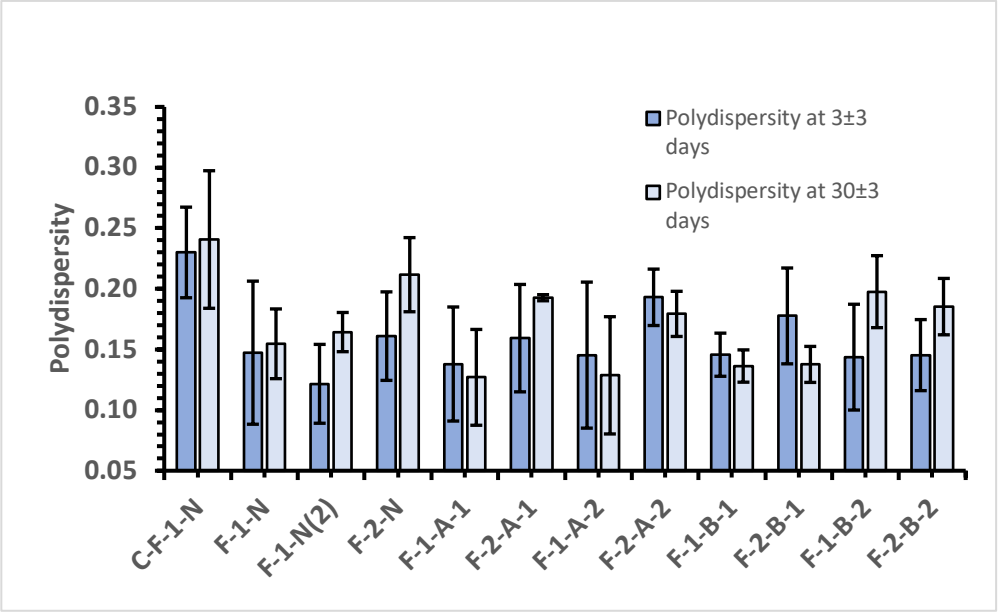


**Figure 4.1.32 - Polydispersity at 3±3 vs 30±3 days**

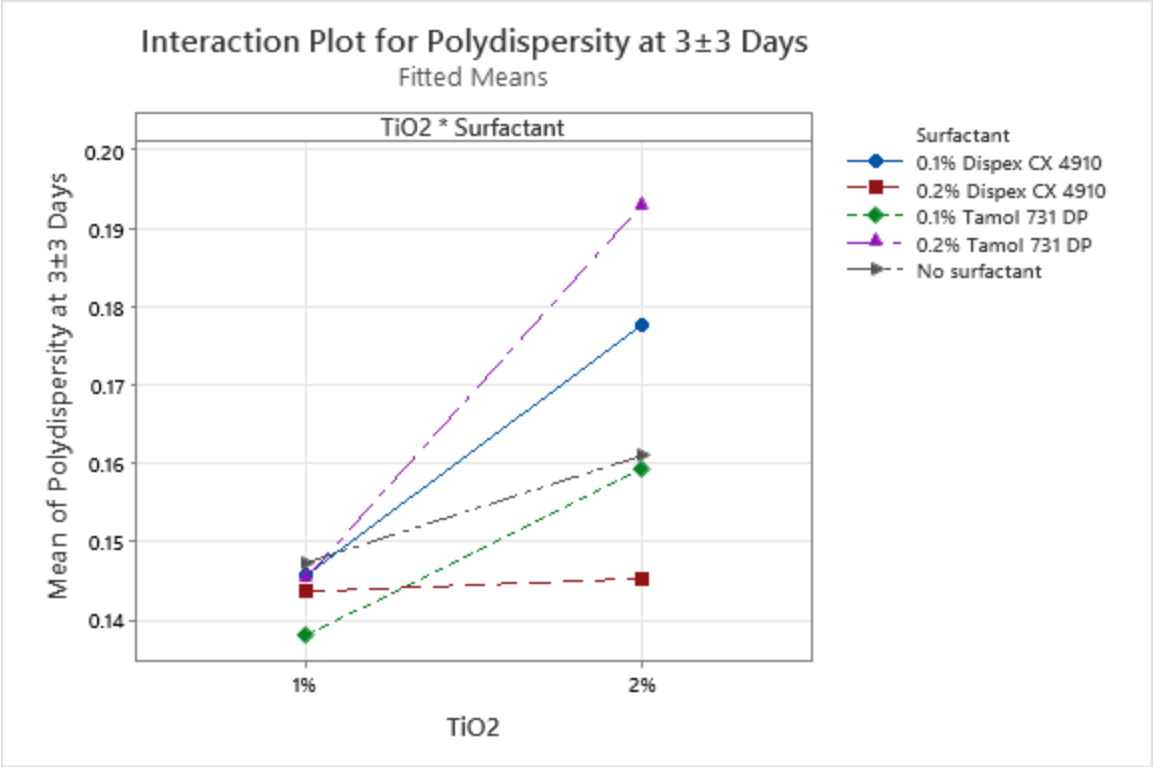


**Figure 4.2.33 – Interaction Plot for Polydispersity at 3±3 Days**

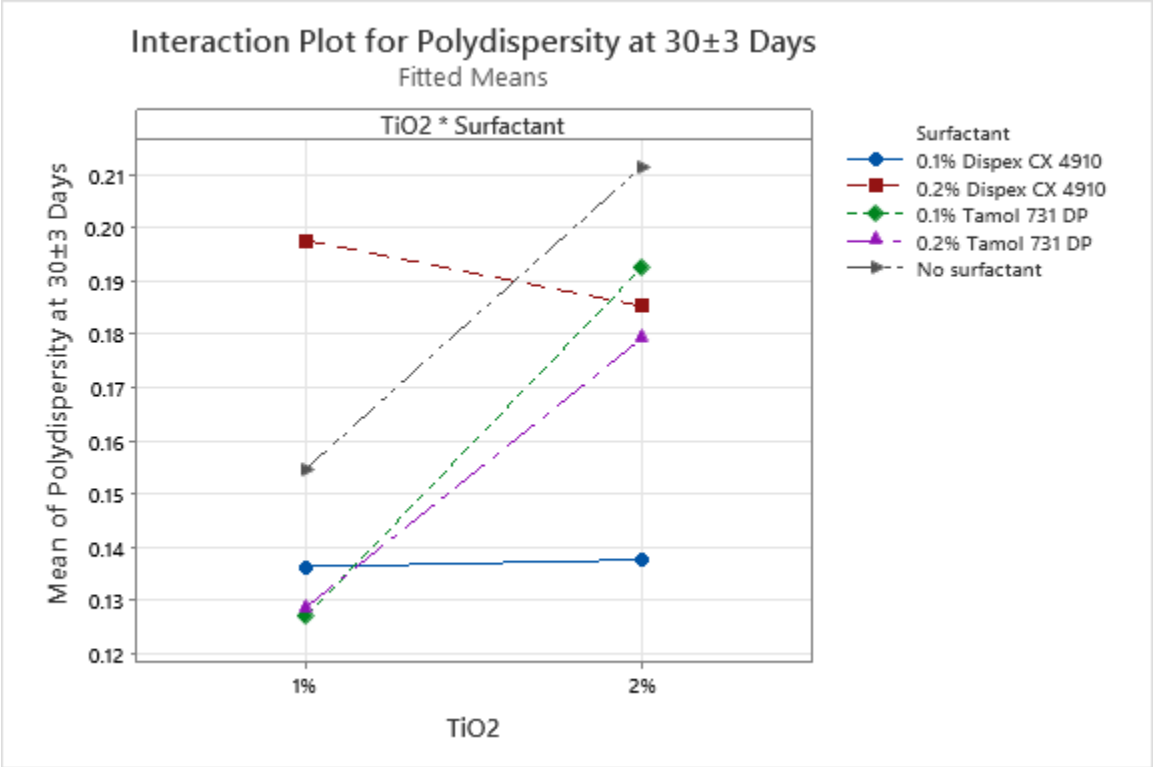


**Figure 4.2.34 – Interaction Plot for Polydispersity at 30±3 Days**

## 4.3 Discussion

The pH values were reported for each sample made, and the pH was not intentionally adjusted. The manufacturer of Aeroxide $TiO_2$ P 25 reports a pH of 3.5 – 4.5 for a 4% dispersion. From the reported data, we can observe that the pH for the four formulas that do not use any surfactant, C-F-1-N, F-1-N, F-1-N(2) and F-2-N is acidic, and varies from 3.984 to 4.106, except for C-F-1-N, Sample B which has a pH value of 4.929. Later on when we discuss the particle size and zeta potential results, it will become apparent that this sample was most likely cross-contaminated and is not a good representation of C-F-1-N. Here, C-F-1-N, F-1-N and F-1-N(2) contained 1 wt.% Aeroxide $TiO_2$ P 25 dispersed in 99 wt.% of 18.2 MΩ water. Formula F-2-N contained 2 wt.% Aeroxide $TiO_2$ P 25 dispersed in 98 wt.% 18.2 MΩ water. From the obtained data, we can conclude that the amount of Aeroxide $TiO_2$ P 25 does not affect the pH significantly.

Formula F-1-A-1, F-2-A-1, F-1-A-2, and F-2-A-2 compositions had an average pH of 10.050, 9.233, 10.518 and 9.840, respectively. These four compositions were stabilized using Tamol 731 DP surfactant. Formula F-1-A-1 and F-2-A-1 contained 1 wt.% and 2 wt.% of Aeroxide $TiO_2$ P 25, respectively dispersed in 0.1 wt.% solution of Tamol 731 DP. Formula F-1-A-2 and F-2-A-2 contained 1 wt.% and 2 wt.% of Aeroxide $TiO_2$ P 25, respectively, dispersed in 0.2 wt.% solution of Tamol 731 DP. From the pH test data, we can conclude that as the amount of Aeroxide $TiO_2$ P 25 is increased from 1 wt. % to 2 wt.%, the pH decreased, considering that the surfactant level was kept constant. Furthermore, as the surfactant level increased from 0.1 wt.% to 0.2 wt.%, the pH increases when the Aeroxide $TiO_2$ P 25 amount is kept constant.

Formula F-1-B-1, as well as F-2-B-1, F-1-B-2 and F-2-B-2 had compositions an average pH of 6.698, 6.787, 6.412 and 6.530, respectively. Formula F-1-B-1 and F-2-B-1 contained 1

wt.% and 2 wt.% of Aeroxide $TiO_2$ P 25, respectively dispersed in 0.1 wt.% solution of Dispex CX 4910. Formula F-1-B-2 and F-2-B-2 compositions contained 1 wt.% and 2 wt.% of Aeroxide $TiO_2$ P 25, respectively dispersed in 0.2 wt.% solution of Dispex CX 4910. From the pH test data we can conclude that as the amount of Aeroxide $TiO_2$ P 25 is increased from 1 wt.% to 2 wt.%, the pH increases, considering the surfactant level was kept constant. Furthermore, as the surfactant level increased from 0.1 wt.% to 0.2 wt.%, the pH decreased when the Aeroxide $TiO_2$ P 25 amount is kept constant.

The calculated theoretical density for 1 wt.% Aeroxide $TiO_2$ P 25 dispersed in 99 wt.% water is 1.008 g/ml and the calculated theoretical density for 2 wt.% Aeroxide $TiO_2$ P 25 dispersed in 98 wt.% water is 1.015 g/ml indicating that as the amount of Aeroxide $TiO_2$ P 25 increases, the density increases too. From the actual data we can see that the average density for the 1 wt.% dispersion varies from 1.002 g/ml to 1.004 g/ml, and for the 2 wt.% dispersion varies from 1.009g/ml to 1.011 g/ml. The slight variation in density between the theoretical and actual could be because of the temperature the samples were tested at, specific gravity of the $TiO_2$ product, exact concentration of the Aeroxide $TiO_2$ P 25 and standard errors. However, based on actual data and theoretical calculations, we can conclude that as the wt.% of Aeroxide $TiO_2$ P 25 increases, the density increases too.

The zeta potential for the compositions that do not contain any surfactant, C-F-1-N, F-1-N, F-1-N(2) and F-2-N, have a positive value, indicating that the charge present on the surface of particles is positive. Here, C-F-1-N, F-1-N and F-1-N(2) all had the same formula, just the manufacturing process was different, and these products have an average zeta potential value of +35.08, +36.25 and +32.00, respectively. F-2-N had an average zeta potential of +38.76.

The zeta potential for the compositions that contain surfactants, have negative value, indicating that the charge present on the surface of the particles is negative. Formulas F-1-A-1, F-2-A-1, F-1-A-2 and F-2-A-2 compositions were stabilized with Tamol 731 DP surfactant and had a zeta potential of -37.06, -27.62, -37.96, and -37.66, respectfully. All the formulae had similar zeta potential values except for F-2-A-1. Further investigation is needed to determine why the absolute zeta potential for this formula is lower than the rest in the series. Formulas F-1-B-1, F-2-B-1, F-1-B-2 and F-2-B-2 compositions were stabilized with Dispex CX 4910 and have a zeta potential of -41.46, -38.38, -47.40 and -44.24, respectively. From research results we can conclude that the absolute zeta potential decreased as the Aeroxide $TiO_2$ P 25 increased from 1 wt.% to 2 wt.%, considering the surfactant was kept constant. Furthermore, it is also apparent that the absolute zeta potential increased when the surfactant increases from 0.1 wt.% to 0.2 wt.%, considering the proportions of Aeroxide $TiO_2$ P 25 was kept constant. Since the zeta potential is a value of measuring the stability of colloid system or dispersion, the higher the absolute value of the zeta potential is, the better the stability of the dispersion is. Typically, zeta potential values of greater than ±30 mV are considered to have sufficient repulsive forces that will give a better stability of the dispersions. This indicates that eleven of the twelve formulae have zeta potential that is greater than ±30 mV, and, therefore, had a good stability. However, it is important to mention that zeta potential on its own is not an ultimate measure for the stability. For example, formula C-F-1-A has a zeta potential of greater than +30 mV which indicates that it has a good stability, where in fact, C-F-1-A had a poor stability, large particle size and hard settlements deposited over investigated time periods.

The effective diameter reported for each sample is an average diameter which is weighted by the light scattered intensity of each particle and corresponds to an average particle size [37].

The polydispersity provides the broadness of the particle size distribution. The particle size and polydispersity were measured initially at 3±3 days and overtime. From the initial test data, we can conclude that formula C-F-1-N had the largest average particle size and broadest particle size distribution. For manufacturing of formula C-F-1-N we did not use the ultrasonic waves after the wetting out of the Aeroxide $TiO_2$ P 25 which end up yielding larger particle size and polydispersity when compared to the other formulation. Furthermore, the representative sample of C-F-1-N had stability issues immediately after dispersing. Here, the sedimentation of the Aeroxide $TiO_2$ P 25 occurred shortly after the dispersion. Overtime, the Aeroxide $TiO_2$ P 25 sediment become hard, and very difficult to disperse in the solution by using gentle agitation. This indicates that ultrasonic waves play a significant role in the stability of the dispersions. The initial average particle size for C-F-1-N was 347.2 nm. However, it is important to mention that Sample B had a higher particle size, as well as different pH and zeta potential when compared to Sample A and C of the same formula C-F-1-N which is indicative of a potential cross-contamination. Therefore, the average particle size of this composition (without Sample B) is 323.1 nm. The initial average polydispersity with Sample B and without Sample B is 0.230 and 0.213, respectively. Excluding Sample B, the average particle size and polydispersity for formula C-F-1-N at 30±3 days is 315.9 nm and 0.208. From the data and the graphs, it is apparent that there is no significant difference between the particle size and polydispersity at 3±3 and 30±3 days, and some difference in values fall within the standard error.

The particle size and polydispersity were tested initially at 3±3 days and then over a period to see the effect of age on the particle size and polydispersity. From the research results, we can observe that the particle size did not increase significantly when compared at 3±3 and 30±3 days for the samples that were produced without a surfactant or with Tamol 731 DP

surfactant. For the samples made with Dispex CX 4910 surfactant, there was no significant difference in particles size, for the samples produced with 0.1 wt.% Dispex CX 4910. Slight increase in particle size was observed for the samples made with 0.2 wt.% Dispex CX 4910 after 30±3 days of storage. The polydispersity for all formulae was between 0.1-0.4, indicating a range of moderate polydisperse distribution.

As discussed above regarding C-F-1-N, one of the objectives of this study was to evaluate whether the wetting out of the Aeroxide $TiO_2$ P 25 by using homogenization can be sufficient for stability. Here, C-F-1-N is of the same theoretical formula as F-1-N and F-1-N(2) but with different manufacturing process. All three formulae had comparable density, pH, and zeta potential. However, there is a significant difference in particle size between C-F-1-N when compared to F-1-N and F-1-N(2). From this data we can conclude that homogenization on its own is not sufficient method to obtain stable dispersions of Aeroxide $TiO_2$ P 25. Furthermore, we wanted to compare whether the method used for wetting out of the Aeroxide $TiO_2$ P 25 played a role in the particle size and stability of the dispersion when the ultrasonic waves were used subsequently. Formula F-1-N was made using the homogenization to wet out the Aeroxide $TiO_2$ P 25, while formula F-1-N(2) was made using mixer with a propeller blade with a diameter that was at least 1/3 of the diameter of the container. All other manufacturing processes were kept consistent. The average particle size for F-1-N and F-1-N(2) samples at 3±3 days was 183.6 nm and 181.3 nm, respectively. The average particles size for F-1-N and F-1-N(2) at 30±3 days was 173.8 nm and 178.3 nm, respectively. The zeta potential for F-1-N and F-1-N(2) was +36.25 and +32.00, respectfully. The density was 1.002 g/ml and 1.003 g/ml for F-1-N and F-1-N(2), respectively; and the pH was 4.089 and 3.996 for F-1-N and F-1-N(2), respectively. From the research data it is apparent that the method used for wetting out the Aeroxide $TiO_2$ P 25 does not

play a significant role in the manufacturing of stable colloidal suspensions when the ultrasonic waves were subsequently used for the dispersion.

# 5. Conclusions

Nanomaterials are of a significant importance for the construction and building industry from the performance and sustainability standpoint. However, it is known that nanomaterials tend to agglomerate via van der Waals forces and aggregate forming solid deposits. Proper dispersions of nanocomponents is essential to realize the expected impacts from application of nanoparticles and obtaining optimum measurable results. This study examined various formulations of titanium dioxide nanoparticles that were stabilized using mechanical energy and ultrasonic waves, and the effect of electrostatic stabilization using anionic surfactants were investigated.

Based on the experimental results, the mechanical energy from homogenization or mixing is not sufficient to develop stable dispersions. Acoustic energy from combination of direct and indirect ultrasonic waves plays significant role in stability, particle size and polydispersity of dispersions, produced from nanoparticles. The method used to wet out the powder nanoparticles, whether it is homogenization or mixing with a propeller blade mixer, did not play a significant role in the stability, particle size or polydispersity of the dispersions when ultrasonic waves were used subsequently.

Dispersions with anionic surfactants, such as Tamol 731 DP and Dispex CX 4910, did not yield a particle size or polydispersity that are significantly different from the dispersions obtained without surfactant, when established manufacturing process was used. However, due to the electrostatic stabilization provided by anionic surfactants, the charge at the surface of the particle changes, and therefore the magnitude and charge of the zeta potential change. Dispersions with Aeroxide $TiO_2$ P 25 that were produced without surfactant have low acidic pH, and positive zeta potential. By using anionic surfactants, the pH of the dispersions was altered,

yielding near neutral pH with one of the surfactants and high alkaline pH with the other, and induced a negative zeta potential. The ability to develop stable dispersions at various pH values is important as this is necessary for application in different sectors, including construction materials and building industry and beyond.

Based on the reported research, the particle size and polydispersity of obtained nanoparticle products did not increase significantly over-time, when ultrasonic waves were used, indicating a good stability as required for practical application. Furthermore, the polydispersity for all dispersions had a moderate polydispersity.

If zeta potential on its own was used as a measure for stability, all formulations, regardless of the manufacturing process, would have exhibit moderate to good stability. Here, the samples that were produced without ultrasonication and characterized by poor stability and sedimentation, had a zeta potential of greater than 30 mV. Even though zeta potential is commonly used as a measure for the stability of dispersions and colloidal systems providing valuable information on the behavior of dispersions, it is important to conclude that the zeta potential on its own cannot determine the stability, and the manufacturing processes play a significant role in the formation of a product with required early and long-term stability.

## Future Work

To see if the particle size can be further reduced to obtain smaller clusters of only few particles with a size of <100 nm, the manufacturing method can be further tuned to accommodate higher intensity of sonic waves, the pH can be adjusted, the amount of the surfactants can be further optimized and reduced, or different, more effective surfactant types can be investigated. Determining the effect of the temperature during manufacturing on the particle size, particle size distribution and stability is another area that should be investigated. Also determining the isoelectric point (IEP) – the pH where a particle does not carry electrical charge, can help establish the mathematical models of the dispersion process and further simplify the formulation process. Depending on the end application of the nanodispersions, and whether these are intended for use as a finished product or as a part of another complex system, it is important to explore the compatibility of developed products with intent substrates or systems. The rheological modifiers to increase the viscosity is another area that can be studied to help reducing the continuous phase viscosity and, therefore, slow down the settlement of nanoparticles overtime. Furthermore, investigating the relationship between various levels of titanium dioxide and surfactant concentrations using multifactorial experimental design models, can provide valuable information on interactions of multiple factors, that are not easily detectable otherwise.

## References


[1] R. P. Feynman, “Plenty of room at the bottom?,” 1959. doi: 10.1511/2012.96.226.

[2] “Nanotechnology Timeline,” *National Nanotechnology Initiative*, 2014.

[3] S. Bayda, M. Adeel, T. Tuccinardi, M. Cordani, and F. Rizzolio, “The history of nanoscience and nanotechnology: From chemical-physical applications to nanomedicine,” *Molecules*, vol. 25, no. 1, pp. 1–15, 2020, doi: 10.3390/molecules25010112.

[4] S. Iijima, “Helical microtubules of graphitic carbon,” *Nature*, vol. 354, pp. 737–740, 1991.

[5] P. Mulvaney, “Nanoscience vs. Nanotechnology-Defining the Field,” *ACS Nano*, vol. 9, no. 3, pp. 2215–2217, 2015.

[6] “What is Nanotechnology ?,” *National Nanotechnology Initiative*, 2016.

[7] N. Baig, I. Kammakakam, W. Falath, and I. Kammakakam, “Nanomaterials: A review of synthesis methods, properties, recent progress, and challenges,” *Materials Advances*, vol. 2, no. 6, pp. 1821–1871, 2021, doi: 10.1039/d0ma00807a.

[8] F. Sanchez and K. Sobolev, “Nanotechnology in concrete - A review,” *Construction and Building Materials*, vol. 24, no. 11, pp. 2060–2071, 2010, doi: 10.1016/j.conbuildmat.2010.03.014.

[9] L. L. Science, “Nanotechnology - New Name-Old Science,” *Lubrizol Life Science*, 2007.

[10] B. Liu and X. Hu, “Hollow Micro- and Nanomaterials: Synthesis and Applications,” in *Advanced Nanomaterials for Pollutant Sensing and Environmental Catalysis*, Elsevier Inc., 2019, pp. 1–38. doi: 10.1016/B978-0-12-814796-2.00001-0.

[11] A. Mohajerani *et al.*, “Nanoparticles in construction materials and other applications, and implications of nanoparticle use,” *Materials*, vol. 12, no. 19, pp. 1–25, 2019, doi: 10.3390/ma12193052.

[12] K. Sobolev and M. F. Gutiérrez, “How nanotechnology can change the concrete world,” *American Ceramic Society Bulletin*, vol. 84, no. 10, pp. 14–18, 2005, doi: 10.1002/9780470588260.ch17.

[13] B. M. Jimmy Law, Abheetinder Brar, “Tyndall Effect,” in *Colloids*, vol. 7, no. 1, 2020, pp. 37–72. [Online]. Available: https://www.researchgate.net/publication/269107473_What_is_governance/link/548173090cf22525dcb61443/download%0Ahttp://www.econ.upf.edu/~reynal/Civil wars_12December2010.pdf%0Ahttps://think-asia.org/handle/11540/8282%0Ahttps://www.jstor.org/stable/41857625

[14] R. J. Hunter, *Foundations of Colloid Science (2nd Edition)*. 2001. [Online]. Available: https://app.knovel.com/web/toc.v/cid:kpFCSE000C/viewerType:toc/root_slug:foundations-of-colloid-science-2nd-edition

[15] S. Mo, X. Shao, Y. Chen, and Z. Cheng, “Increasing entropy for colloidal stabilization,” *Scientific Reports*, vol. 6, pp. 1–7, 2016, doi: 10.1038/srep36836.

[16] U. of Washington, “Electrostatic Stabilization,” *University of Washington*.

[17] M. Instruments, “Zeta Potential-Introduction in 30min,” *Malvern Instruments*, 2015.

[18] U. Nobbmann, “Debye screening - how it affects zeta potential,” *Malvern Panalytical*, 2018.

[19] M. Kaszuba, J. Corbett, F. M. N. Watson, and A. Jones, “High-concentration zeta potential measurements using light-scattering techniques,” *Philosophical Transactions of*

*the Royal Society A: Mathematical, Physical and Engineering Sciences*, vol. 368, no. 1927, pp. 4439–4451, 2010, doi: 10.1098/rsta.2010.0175.
[20] A. Sze, D. Erickson, L. Ren, and D. Li, "Zeta-potential measurement using the Smoluchowski equation and the slope of the current-time relationship in electroosmotic flow," *Journal of Colloid and Interface Science*, vol. 261, no. 2, pp. 402–410, 2003, doi: 10.1016/S0021-9797(03)00142-5.
[21] P. M. v Raja and A. R. Barron, "Zeta potential analysis," in *Physical methods in chemistry and nano science*, 2021. doi: 10.1002/jctb.5000533702.
[22] D. H. Napper, "Colloid Stability," *Industrial and Engineering Chemistry Product Research and Development*, vol. 9, no. 4, pp. 467–477, 1970, doi: 10.1021/i360036a005.
[23] S. Karmakar, "Particle Size Distribution and Zeta Potential Based on Dynamic Light Scattering: Techniques to Characterize Stability and Surface Charge Distribution of Charged Colloids," *Recent Trends in Materials: Physics and Chemistry*, no. January, pp. 117–159, 2019.
[24] G. Trefalt and M. Borkovec, "Overview of DLVO Theory," 2014. [Online]. Available: www.colloid.ch/dlvo
[25] M. Danaei *et al.*, "Impact of particle size and polydispersity index on the clinical applications of lipidic nanocarrier systems," *Pharmaceutics*, vol. 10, no. 2, pp. 1–17, 2018, doi: 10.3390/pharmaceutics10020057.
[26] "Dynamic Light Scattering ( DLS ) Particle Size Distribution Analysis," *Horiba Scientific*.
[27] U. Nobbmann, "Polydispersity-what does it mean for DLS and chromatography?," *Malvern Panalytical*, 2017.
[28] I. M. Mahbubul *et al.*, "Effect of ultrasonication duration on colloidal structure and viscosity of alumina-water nanofluid," *Industrial and Engineering Chemistry Research*, vol. 53, no. 16, pp. 6677–6684, 2014, doi: 10.1021/ie500705j.
[29] M. M. Islam, *Preparation, Characterization, Properties, and Application of Nanofluid*. Elsevier Inc., 2018. doi: 10.1016/b978-0-12-813245-6.00009-5.
[30] R. Sadeghi, S. G. Etemad, E. Keshavarzi, and M. Haghshenasfard, "Investigation of alumina nanofluid stability by UV–vis spectrum," *Microfluidics and Nanofluidics*, vol. 18, no. 5–6, pp. 1023–1030, 2015, doi: 10.1007/s10404-014-1491-y.
[31] M. H. Samat, A. M. M. Ali, M. F. M. Taib, O. H. Hassan, and M. Z. A. Yahya, "Hubbard U calculations on optical properties of 3d transition metal oxide TiO2," *Results in Physics*, vol. 6, pp. 891–896, 2016, doi: 10.1016/j.rinp.2016.11.006.
[32] M. Monai, T. Montini, and P. Fornasiero, "Brookite: Nothing new under the sun?," *Catalysts*, vol. 7, no. 10, 2017, doi: 10.3390/catal7100304.
[33] K. Nakata and A. Fujishima, "TiO 2 photocatalysis: Design and applications," *Journal of Photochemistry and Photobiology C: Photochemistry Reviews*, vol. 13, no. 3, pp. 169–189, 2012, doi: 10.1016/j.jphotochemrev.2012.06.001.
[34] T. Ohno, K. Sarukawa, K. Tokieda, and M. Matsumura, "Morphology of a TiO2 photocatalyst (Degussa, P-25) consisting of anatase and rutile crystalline phases," *Journal of Catalysis*, vol. 203, no. 1, pp. 82–86, 2001, doi: 10.1006/jcat.2001.3316.
[35] S. H. Othman, S. Abdul Rashid, T. I. Mohd Ghazi, and N. Abdullah, "Dispersion and stabilization of photocatalytic TiO 2 nanoparticles in aqueous suspension for coatings applications," *Journal of Nanomaterials*, vol. 2012, 2012, doi: 10.1155/2012/718214.

[36] D. M. Tobaldi, R. C. Pullar, M. P. Seabra, and J. A. Labrincha, “Fully quantitative X-ray characterisation of Evonik Aeroxide TiO 2 P25®,” *Materials Letters*, vol. 122, pp. 345–347, 2014, doi: 10.1016/j.matlet.2014.02.055.
[37] Brookhaven Instruments Corporation, “Zeta Plus Zeta Potential Analyzer .” Brookhaven Instrument Corporation, Jun. 2003.